frontiers | Frontiers in Energy Research

ORIGINAL RESEARCH
published: 14 July 2022
doi: 10.3389/fenrg.2022.902776

Robust Load Frequency Control of Hybrid Solar Power Systems Using Optimization Techniques

Syed Mahboob Ul Hassan, Makbul A. M. Ramli and Ahmad H. Milyani*

Department of Electrical and Computer Engineering, King Abdulaziz University, Jeddah, Saudi Arabia

It is necessary to predict solar photovoltaic (PV) output and load profile to guarantee the security, stability, and reliability of hybrid solar power systems. Severe frequency fluctuations in hybrid solar systems are expected due to the intermittent nature of the solar photovoltaic (PV) output and the unexpected variation in load. This paper proposes designing a PID controller along with the integration of a battery energy storage system (BESS) and plug-in hybrid electric vehicle (PHEV) for frequency damping in the hybrid solar power system. The solar PV output is predicted with high accuracy using artificial neural networks (ANN) given that solar irradiance and cell temperature are inputs to the model. The variation in load is also forecasted considering the factors affecting the load using ANN. Optimum values of the PID controller have been found using genetic algorithm, particle swarm optimization, artificial bee colony, and firefly algorithm considering integral absolute error (IAE), integral square error (ISE), and integral time absolute error (ITAE) objective functions. IAE, ISE, ITAE, Rise time, settling time, peak overshoot and maximum frequency deviation have been measured for comparison and effectiveness. The transient behavior has been further improved by utilizing the power from BESS/PHEV to the power system. The results demonstrate the efficacy of the suggested design for frequency control using the genetic algorithm method along with ISE objective function compared with those obtained from the conventional, particle swarm optimization, artificial bee colony, and firefly algorithm techniques.

Keywords: load frequency control, PID controller design, load deviation forecasting, solar photovoltaic power forecasting, particle swarm optimization, genetic algorithm, artificial bee colony (ABC) algorithm

OPEN ACCESS

Edited by:
Chuan-Ke Zhang,
China University of Geosciences Wuhan, China

Reviewed by:
D. Boopathi,
Paavai Engineering College, India
Hazlie Mokhlis,
University of Malaya, Malaysia

****Correspondence:***
Syed Mahboob Ul Hassan
mahboobulhassan145@gmail.com
sulhassan@stu.kau.edu.sa

Specialty section:
This article was submitted to Smart Grids, a section of the journal Frontiers in Energy Research

Received: *23 March 2022*
Accepted: *04 May 2022*
Published: *14 July 2022*

Citation:
Mahboob Ul Hassan S, Ramli MAM and Milyani AH (2022) Robust Load Frequency Control of Hybrid Solar Power Systems Using Optimization Techniques. Front. Energy Res. 10:902776. doi: 10.3389/fenrg.2022.902776

INTRODUCTION

Solar photovoltaic (PV) systems are intermittent in nature. The variation in generated power and load demand is common in solar PV connected power systems. Under normal operating situations, microgrids are powered by the integration of both solar PV systems and the power grid. However, when the output from the solar PV system is lower than expected, and the load demand is high, the power grid may not be able to support enough power because of its slow dynamic response. This will cause the power system to be unstable which leads to severe frequency fluctuations in the system (Sadat, 2012).

Hybrid solar power systems are a source for generating electrical power that use inverters coupled with batteries to store energy later use. In this way, hybrid solar systems will be able to use the stored energy during blackouts and compensate for renewable energy sources output fluctuation (Newkirk, 2015). Integrating microgrids with renewable energy systems is considered an adequate solution to

meet the increasing demand of electric power. Such microgrids can utilize plug-in hybrid electric vehicles and battery energy storage systems to maintain the balance between generated power and the load demand. Due to the intermittent nature of renewable energy sources, the change in generation power and load demand would lead the system to instability causing severe frequency fluctuations. Mathematical models were developed to predict the behavior of microgrids in order to dampen frequency fluctuations. Power systems with a high penetration of renewable energy sources were integrated with battery energy storage system (BESS) and plug-in hybrid electric vehicles to maintain the frequency deviations within limits (Akula, 2019).

Mellit (Mellit and Pavan, 2010) uses artificial neural network methods for forecasting the electric power produced by a 20 kW_p grid-connected PV system placed on a rooftop in the municipality of Trieste, Italy. According to Huang (Huang et al., 2016), improved the solar photovoltaic (PV) output by using the solar irradiance and temperature along solar zenith angle and solar azimuth angle with the help of artificial neural network methods. A data-driven ensemble approach was used by Al-Dahidi in (Al-Dahidi et al., 2019) to predict the day ahead solar photovoltaic (PV) output (230 kW_{ac} capacity) placed on the top of the Applied Science Private University, Amman, Jordan to overcome the intermittent nature of solar energy system.

Hote (2018) studied the PID controller calibrating approaches for load frequency control of Power systems. The prime challenge in LFC was to design a PID controller that could maintain the frequency fluctuations rigorously within the defined limits. Fractional Order PID controller was tuned by Taher (2014) for load frequency control for three area power system with the help of imperialist competitive algorithm (ICA). The response of the interconnected power system towards disruption was smooth and less vibratory as a result of using the proposed controller. Mosaad (Mosaad and Salem., 2014) presented a methodological design for an adaptive PID load frequency using artificial neural networks (ANN) and adaptive Neuro-Fuzzy Inference systems (ANFIS). The PID Controller was able to maintain the effective performance at any load point in the power system with the superiority of ANFIS over ANN with respect to integral absolute error (IAE), integral square of errors. According to Otani (2017), there are possible chances of frequency fluctuations after losing balance between power generated and load demand. Battery storage was incorporated because of its faster response to overcome load frequency deviations using recurrent neural networks.

The desired frequency of the power system deviates due to disturbances in the electric power generation and load fluctuations. Load frequency control has been considered the main issue for power system operation and control for effective and reliable power supply (Sundaram and Jayabarathi, 2011). PI, PID and fuzzy controllers have been used to stabilize the power system when it is integrated with wind power. Kumari et al. (2016) introduce the ANN-based PID controller to sufficiently damp frequency fluctuations produced as a result of load changes. An artificial intelligent controller has been designed using the backpropagation algorithm to reduce the area control error of a two-area hydrothermal power system for automatic generation control purposes in (Rao, 2012).

Meta-heuristic optimization techniques have been employed to get the optimal gains of PID controller for LFC problem. According to (Das et al., 2010), genetic algorithm based PID controller was tuned for autonomous hybrid generation system. Fractional order PID controller was tuned using genetic algorithm for hybrid power system integrated with renewable energy sources (Regad et al., 2019). Multi-objective artificial bee colony technique was adopted to tune the PID controller parameters with the help of integral time multiplied absolute error (ITAE) and integral of time weighted squared error (ITSE) for two area thermal power system (Naidu et al., 2014). Particle swarm optimization has been utilized to tune the fuzzy logic controller for the frequency restoration of multi-area power system (Jaber et al., 2013). PSO is used for obtaining the optimal PID parameters for two area system with integral square error as cost function and showing best convergence profile (Nagarjuna and Shankar, 2015). PID optimal parameters obtained for two and three area power system using firefly algorithm considering the generation rate constraint and governor dead band (Padhan et al., 2014).

Energy storage systems are also used in previous studies for frequency regulation. The role of battery energy storage system has been presented for regulating the frequency in interconnected power system. The results are compared to the conventional PID controller that describe BESS as efficient for LFC purpose (Kalyani et al., 2012). Peak frequency deviation and settling time of two area power system is reduced using the battery energy storage system and choosing the proper integral gain (Aditya and Das, 2001). Plug-in electric vehicles power is utilized for frequency stability of the islanded power system with the help of controllable power rate strategy (Qi et al., 2018). The energy from electric vehicles that are charged during daytime can be utilized in the night-time for small residential power system (Takagi et al., 2009).

The purpose of this study to address the limitations in the previous studies and fulfill the gap. Many load frequency control techniques have been applied to power system for its stability purposes, i.e., robust control, decentralized aspect, linear quadratic, pole shifting, and variable structure. But there have been some drawbacks of these techniques which decrease their execution efficiency. To overcome such problem, artificial intelligence techniques, fuzzy logic (FL) and neural network (NN) have been adopted and applied to solve the non-linear models of the power system. These techniques have proved their effectiveness and efficiency to solve the problem. But they still have some disadvantages. For example, it is hard to train the neural network again and again to set the number of neurons and other parameters to get the best output response. Similarly, fuzzy logic requires hard work to get the influential signal response from the power system (Abd-Elazim and Ali, 2018). Optimization techniques such as genetic algorithm (GA) (Milani and Mozafari, 2009) (Chang et al., 1998; Rerkpreedapong et al., 2003; Das et al., 2010; Das et al., 2012; Mallesham et al., 2012; Konar et al., 2014; Regad et al., 2019; Hemeida et al., 2020; Sidi Brahim et al., 2021), particle swarm

optimization (PSO) (Pain and Acharjee, 2014; Abd-Elazim and Ali, 2018) (Gözde et al., 2008; Selvakumaran et al., 2012; Modi et al., 2013; Rao and Rama Krishna Reddy, 2015; Shankar et al., 2015; Hazlee Azil et al., 2016; Jeyalakshmi and Subburaj, 2016; Singh and Ramesh, 2019; Hemeida et al., 2020; Veerasamy et al., 2020; Safari et al., 2021) (Sidi Brahim et al., 2021) (Mallesham et al., 2012)- (Kumari and Jha, 2014), firefly algorithm (FA) (Naidu et al., 2013; Shakarami et al., 2013; Padhan et al., 2014; Chandra Sekhar et al., 2016; Abd-Elazim and Ali, 2018; Boddepalli and Navuri, 2018; Gupta et al., 2021), and artificial bee colony (Ghasemi and Shayeghi, 2011; Rathor et al., 2011; Gozde et al., 2012; Naidu et al., 2014; Elsisi et al., 2015; Kouba et al., 2015; Kumar et al., 2017; Abo-Elyousr, 2018), have been used and found to be effective for load frequency control problem. But proportional, integral and derivative gain range of PID controller during optimization problem has been narrowed. Renewable energy source, photovoltaic and wind turbine, transfer function model has been adopted in the previous studies. In the same way, load frequency control has also been done in previous studies using the energy storage systems but without efficient PID controller that ultimately require large energy storage capacity to damp the frequency (Kalyani et al., 2012)- (Aditya and Das, 2001). Taking into account the mentioned limitations, the current study discusses and solve the problem by taking real-time data to train the network for solar photovoltaic prediction, load deviation forecasting, widening proportional, integral, and derivative controller gain range, and integrating the BESS/PHEV with efficient tuned PID controller.

The major contributions of this paper are threefold and shown below.

1) Solar photovoltaic generated power and load deviation have been forecasted from the affecting factors using artificial neural networks.
2) The forecasted solar photovoltaic power and load deviation have been utilized by the power system model to find the optimal PID controller parameters using genetic algorithm, particle swarm optimization, artificial bee colony and firefly algorithm optimization techniques considering the integral absolute error, integral square error, and integral time absolute error objective functions.
3) BESS/PHEV model, with gain levels 10 and 50 respectively, has been integrated to the power system model to further dampen the frequency deviation.

POWER SYSTEM MODEL

Power system control concentrate on steady state operation. This study presents how to deal with active power to keep the power system in steady state. The major objective of the control strategy is to provide qualitative and reliable power to customers within an interconnected system. Changes in the active power disturb the frequency of the system. Therefore, a control strategy is designed to regulate load frequency control using control loops. Two common approaches, transfer function and state variable, are adopted to transform the power system model into a mathematical model by making some proper assumptions (Prakash and Sinha, 2012; Pain and Acharjee, 2014; Prajapati and Parmar, 2016; Azeer et al., 2017; Lone et al., 2018; Yang-Wu et al., 2019). A single area power system model is shown in **Figure 1**.

Generator Model

The generator equation has been extracted from the swing equation as shown in **Eq. 1**.

$$\Delta\omega(s) = \frac{1}{2Hs}\left[\Delta P_m(s) + \Delta P_{PV}(s) - \Delta P_e(s)\right] \tag{1}$$

Load Model

The power system contains resistive and inductive load that is frequency independent and dependent respectively (Sadat, 2012). Therefore, the net change in load power can be described as the combination of frequency sensitive and frequency non-sensitive load changes shown in **Eq. 2**.

$$\Delta P_e(s) = \Delta P_L + D\Delta\omega \tag{2}$$

Where ΔP_L is the frequency independent load change and $D\Delta\omega$ denotes the frequency-sensitive load change and D represent the ratio of percent change in load to the percent change in frequency. So, the relationship for variation in load with respect to frequency fluctuation can be expressed as,

$$\Delta P_{L(freq)} = D\Delta\omega \text{ or } D = \frac{\Delta P_{L(freq)}}{\Delta\omega} \tag{3}$$

Many factors affect the electric load (Khatoon and Singh, 2014). These factors could be short term, middle term, and long-term influence factors. Some important factors used for load forecasting are categorized as follows.

- Meteorological factors involving temperature, wind speed, humidity, surface pressure, and precipitation factor are responsible for load forecasting.
- Temporal or calendar factors involving hour of the day and day of the week.
- Random factors such as sports activities.

Frequency dependent load change has been observed from the Atlas Power Plant. The Atlas power plant is a coal fired thermal power plant located at the geographic location (Longitude: 31.5204, Latitude:74.3587). The historical load demand data has been extracted from the power data reference book produced by the National Transmission and Dispatch Company Limited (NTDCL) (Power Data Reference Book, 2017). Historical daily load data from 2011 to 2016 has been taken as input along with weather and seasonal data. Seasonal and weather data consists of wind speed, surface pressure, temperature, precipitation factor, and humidity. Average load has been calculated for 365 days from load profile data between 2011 and 2016 (Alessandra et al., 2011). Frequency dependent change in load has been extracted from the average load for

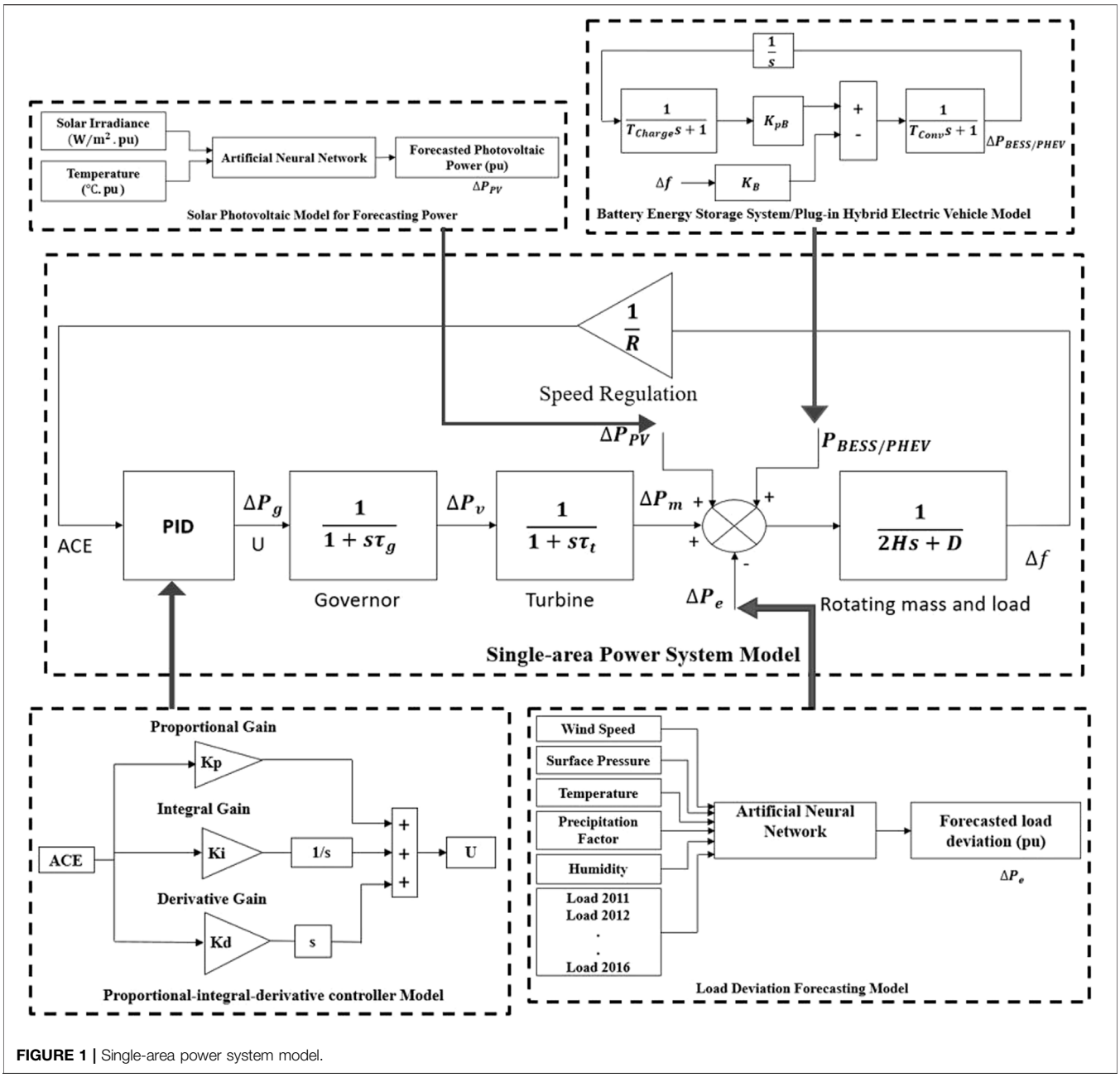

FIGURE 1 | Single-area power system model.

consecutive 365 days as shown in **Figure 2**. This change in load power has been taken as an output (Kotur and Žarković, 2016).

The weather data has been first normalized by taking the maximum value as base from each factor affecting the load and dividing the entirety of the weather data with base value within the range (0–1). Similarly, historical data has also been normalized by dividing with the base value 219 MW and converting the load data within the range of (0–1). After normalizing the input and target data, NNTOOL is used to train the network. A multi-layer feed forward neural network was trained using wind speed, surface pressure, temperature, precipitation factor, humidity, and historical load data as input and deviation in load power data as target as shown in **Figure 1** of the load deviation model (Srinivasan et al., 1991). The number of neurons has been chosen as 10, Tan sigmoid activation function, and Levenberg Marquardt as learning algorithm as shown in **Table 1**. The trained model depicts its effectiveness showing the coefficient of regression as 1.0 and mean squared error (MSE) as 1.68×10^{-16} at 525 epochs. After training model, the network model was deployed in Simulink, where the neural network can successfully forecast the deviation in load power.

Prime Mover Model

It is the origin of mechanical power whose energy is obtained from burning coal or gas, or nuclear fission. The transfer function of the turbine can be represented as the ratio of the change in

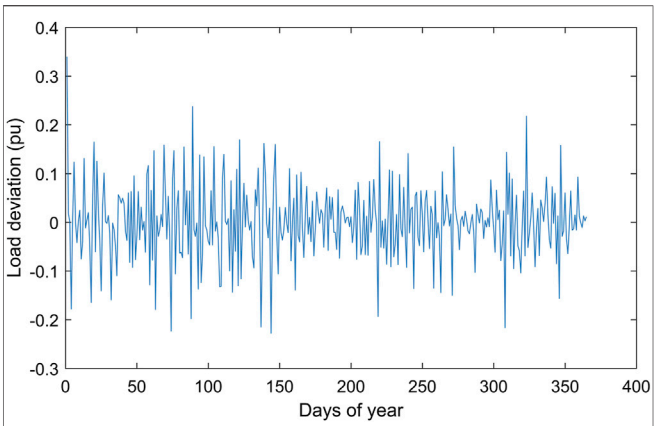

FIGURE 2 | Load deviation of power system for one-year period.

mechanical output power $\Delta P_m(s)$ to the change in steam valve position $\Delta P_v(s)$ as represented by **Eq. 4**.

$$G_T(s) = \frac{\Delta P_m(s)}{\Delta P_v(s)} = \frac{1}{1 + s\tau_t} \tag{4}$$

Where τ_t is the turbine time constant.

Governor Model

The speed governor model can be expressed as **Eq. 5.**

$$\Delta P_g(s) = \Delta P_{ref} - \frac{1}{R}\Delta\omega(s) \tag{5}$$

The speed governor operates as a comparator and its output ΔP_g can be written as difference between the reference set power ΔP_{ref} and power $\frac{1}{R}\Delta\omega$, where R indicates the speed regulation. The relation between governor input and valve opening can be expressed by **Eq. 6** (Kumari et al., 2016).

$$\Delta P_v(s) = \frac{1}{1 + s\tau_g}\Delta P_g(s) \tag{6}$$

Where τ_g is taken as the governor time constant in seconds.

Solar Photovoltaic Model

It is fact that photovoltaic output power is intermittent in nature. It depends on two main factors: solar irradiance and temperature (Rodríguez et al., 2018). Solar photovoltaic power is directly proportional to solar irradiance while inversely proportional to temperature (Abd-Elazim and Ali, 2018). Solar photovoltaic model of 5 MW is considered at location (Longitude:31.5204, Latitude:74.3587) near the thermal power plant. Solar PV system is integrated to the thermal power plant. The solar power plant is built by LONGI solar modules of power 540W. LONGI solar module characteristics are shown in **Table 2**. The solar PV module output (W) was considered at different solar irradiance (ranges 100–1100 W/m^2) and temperature (0°C–55°C). These changes were applied to the whole 5 MW power plant to see the effect of intermittency on the power plant. The solar PV generated power 5 MW has been normalized using the base power of 219 MW according to the thermal power plant. A multi-layer feed forward neural network was trained using solar irradiance and temperature as input data and solar power as target data (Sedaghati et al., 2012; Ncane and Saha, 2019). The number of neurons is chosen to be 10, Tan sigmoid activation function, and Levenberg Marquardt as learning algorithm as shown in **Table 3**. The trained model depicts its effectiveness showing the coefficient of regression as 1.0 and mean squared error as 8.4×10^{-10} at epochs 22. After successfully training the model, the network model was deployed using Simulink, where neural network can successfully forecast the solar power using the input data taken from the National Aeronautics and Space Administration (NASA). The peak value of solar irradiance and its corresponding temperature at a specific time of the day is considered to forecast the solar photovoltaic output power for that day.

Battery Energy Storage System/Plug-in Hybrid Electric Vehicle Model

Energy storage systems are a great source of frequency damping in the power system. As discussed in the introduction section, power from battery energy storage systems and plug-in hybrid electric vehicle play an important role for maintaining the frequency. Energy from PHEV can be utilized for small residential systems. The circle of willingness of customers for utilizing PHEV can be enhanced. **Figure 1** consists of the control system model for a battery energy storage system or plug-in hybrid electric vehicle integrated to the power system. The term $\frac{K_{pB}}{T_{charge}S+1}$ depicts the mechanism of auto balancing charging loop. This close-loop control will maintain the energy of the BESS/PHEV near the initial state, which is considered 50% charged. K_B is the feedback gain from the frequency fluctuation in the power grid. $\frac{1}{T_{Conv}S+1}$ represent the first order conversion delay from DC to AC of the BESS/PHEV (Uehara et al., 2009; Liang et al., 2012).

TABLE 1 | Summary of artificial neural network design and architecture for forecasting load deviation.

Network type	Multi-layer feedforward neural network
Inputs	6 inputs- wind speed, surface pressure, temperature, precipitation factor, humidity, historical load 2011–2016
Outputs	1 output-deviation in load
Number of layers	Input, hidden, output
Number of hidden neurons	10
Activation function	Tan-sigmoid, linear
Learning algorithm	Levenberg-Marquardt

TABLE 2 | Electrical characteristics of LONGI Solar 540W module.

Module type	LR5-72HPH-540M	
Testing condition	**STC:AM1.5, 1000 W/m², 25 ℃**	**NOCT:AM1.5, 800 W/m², 20 ℃**
Maximum power (P_{max}/W)	540	403.3
Open circuit voltage (V_{oc}/V)	49.50	46.41
Short circuit current (I_{sc}/A)	13.85	11.20
Voltage at maximum power (V_{mp}/V)	41.65	38.78
Current at maximum power (I_{mp}/A)	12.97	10.40
Module efficiency (%)	21.1	

TABLE 3 | Summary of artificial neural network design and architecture for forecasting solar photovoltaic power.

Network type	Multi-layer feedforward neural network
Inputs	2 inputs- solar irradiance, temperature
Outputs	1 output-module power
Number of layers	Input, hidden, output
Number of hidden neurons	10
Activation function	Tan-sigmoid, linear
Learning algorithm	Levenberg-Marquardt

PID Controller Model for Optimization Problem

The PID Controller model has been adopted in the power system model as shown in **Figure 1**. The transfer function of the controller is as follows.

$$G_{PID}(s) = K_p + \frac{K_i}{s} + K_d s \tag{7}$$

The control signal for maintaining the system frequency is given by **Eq. 8** (Abd-Elazim and Ali, 2018).

$$U(s) = -G_{PID}(s) \times ACE(s) \tag{8}$$

where ACE is the area control error of the power system and U is the input signal to the governor for controlling the valve output according to load demand of the power system.

Area Control Error (ACE) of studied single-area power system can be written by **Eq. 9**.

$$ACE = B \times \Delta\omega \tag{9}$$

B is called bias factor and denoted with $B = \frac{1}{R} + D$, and $\Delta\omega$ represents the frequency deviation.

Multi-objective function is used in (Naidu et al., 2014) for load frequency control using the artificial bee colony optimization approach considering ITAE and ITSE. It has been observed the performance of the PID controller can be compromised, i.e., Either frequency deviation or settling time is compromised on the cost of each other. Therefore, it is recommended to use objective functions separately. But, the most suitable objective function should be identified based on the performance indices and convergence profile.

Three objective functions J are used to check the performance indices of the PID controller, which are the integral absolute error (IAE), integral square error (ISE), and integral time absolute Error (ITAE) and given by **Eqs 10–12**.

$$J_{IAE} = \int_{-\infty}^{\infty} |e(t)| dt \tag{10}$$

$$J_{ISE} = \int_{-\infty}^{\infty} e(t)^2 dt \tag{11}$$

$$J_{ITAE} = \int_{-\infty}^{\infty} t*|e(t)| dt \tag{12}$$

Where $e(t)$ is area control error (ACE).

Frequency deviation permissible limit is calculated using the following steady-state equation (Sadat, 2012).

$$\Delta\omega_{ss} = \frac{\pm \Delta P_L}{\frac{1}{R} + D} \tag{13}$$

The maximum steady-state frequency deviation in Hz has found to be −0.7932 Hz for maximum positive load change and 0.5468 Hz for maximum negative load change for studied model. So, the frequency deviation permissible limit range should be (−0.7932, 0.5468) in Hz.

PROPOSED APPROACHES FOR TUNING THE PID CONTROLLER

Particle Swarm Optimization

Particle swarm optimization technique was developed by Kennedy and Eberhart in 1995. They used nature inspired optimization algorithms in their technique. In this technique, particles are flown through the search space and update the position of the i_{th} particle at time step of t. The expression for the velocity updates is given by the **Eq. 14**.

$$v_i(t+1) = \omega v_i(t) + c_1 rand_1 \cdot \left(pbest_i - x_i(t)\right) + c_2 rand_2 \cdot \left(gbest_i - x_i(t)\right) \tag{14}$$

This technique is adopted to find the optimal values of the PID controller parameters. Initially, the PID controller proportional gain K_p, integral gain K_i, and derivative gain K_d optimal values have been searched in the range (−10, 1000). The searched controller gains produce insufficient closed-loop stability of the power system in this range. Therefore, the gain parameters range has been narrowed iteratively until closed-loop stability condition of power system model is achieved within the range

TABLE 4 | Meta-heuristic techniques operators used to find out optimal PID gain parameters.

Option	Number/Type
Genetic algorithm	
Number of variables	3
Limit	(−10, 150)
Population size	Default, 50
Creation function	Uniform
Fitness scaling function	Rank
Selection function	Tournament
Crossover fraction	Default, 0.8
Mutation function	Adaptive feasible
Crossover function	Arithmetic
Fitness function	IAE, ISE, ITAE
Stopping criteria	Default, 100*Number of variables
Particle swarm optimization	
No. of variables	3
No. of particles	30
No. of iterations	50
Objective functions	IAE, ISE, ITAE
Limit	(−10, 150)
$C_1 = C_2$	2
w_{max}	0.9
w_{min}	0.4
Artificial bee colony	
No. of populations	30
No. of iterations	60
Number of variables	3
Objective functions	IAE, ISE, ITAE
Limit	(−10, 150)
a (acceleration coefficient)	1
Number of onlooker bees	30
Firefly algorithm	
No. of populations	30
No. of iterations	50
Number of variables	3
Objective functions	IAE, ISE, ITAE
Limit	(−10, 150)
γ	1
β	1
α	0.2
ε	0.98

(−10, 150). PID controller produces best results and minimizes the error significantly within the selected range (−10, 150) as compared to very short range (0, 5) (Pain and Acharjee, 2014; Abd-Elazim and Ali, 2018) (Gözde et al., 2008; Selvakumaran et al., 2012; Modi et al., 2013; Rao and Rama Krishna Reddy, 2015; Shankar et al., 2015; Hazlee Azil et al., 2016; Jeyalakshmi and Subburaj, 2016; Singh and Ramesh, 2019; Hemeida et al., 2020; Veerasamy et al., 2020; Safari et al., 2021) (Sidi Brahim et al., 2021) (Mallesham et al., 2012)- (Kumari and Jha, 2014). **Table 4** depicts the PSO operators used to find out the optimal PID controller parameters. The best performing PID controller parameters are mentioned in **Table 5**.

Genetic Algorithm

Genetic Algorithm is an optimization technique based on heredity and evolution. This technique was suggested by John Holland in 1960 to search for the best solution of complex problems. It is an iterative process which maintains the constant population size of desired solution. GA initially begins with a randomly selected population of function input that is represented as a bit of strings. The Population is evaluated in each iterative step called generations to give a new population of the desired solution. That means GA uses the current population to produce a new population such that the new population is better on average if compared to the previous population. Best elements are used from the current population to form the best population. The successful process will produce a population better than the old one. Three steps selection, mating, and mutation are used to produce new population from the old population. The basic genetic algorithm cycle is shown in **Figure 3**. New generations are produced iteratively with the repetition of these three steps. The process continues until the stopping criteria is reached like the maximum number of iterations is achieved or no improvements (Milani and Mozafari, 2009) (Chang et al., 1998; Rerkpreedapong et al., 2003; Das et al., 2010; Das et al., 2012; Mallesham et al., 2012; Konar et al., 2014; Regad et al., 2019; Hemeida et al., 2020; Sidi Brahim et al., 2021).

This technique is adopted to find the optimal values of the PID controller parameters. The PID controller proportional gain K_p, integral gain K_i, and derivative gain K_d optimal values have been searched in the range (−10, 150). Different parameters and functions for applying GA technique are used in OPTIMTOOL toolbox of MATLAB and given in **Table 4**. The optimal parameters obtained are depicted in **Table 5**.

Firefly Algorithm

The flashing light of fireflies is of great importance to study their pattern and rhythmic movement. Studies discussed the main aim of pattern of flashes is either to communicate with the mating partners, to attract the potential prey or to signal other fireflies for potential safety warning. This signal consists of rhythmic flash, rate of flash and amount of flashing. This behavior of flashing light from fireflies can be used to solve many optimization problems. This algorithm has been developed by Xin-She Yang in 2008.

The Euclidian distance r_{ij} between two fireflies i and j with respect to their positions x_i and x_j can be found with the flowing **Eq. 15**

$$r_{ij} = \sqrt{\sum_{k=1}^{d} \left(x_{i,k} - x_{j,k}\right)^2} \tag{15}$$

Where k denotes the kth element of the geographical coordinates. The attractiveness between fireflies can be denoted with the following attractiveness parameter.

$$\beta = \beta_0 e^{-\gamma r^2} \tag{16}$$

TABLE 5 | PID controller gain parameters using IAE, ISE, and ITAE objective function.

PID gain parameters	IAE			ISE			ITAE		
	K_p	K_i	K_d	K_p	K_i	K_d	K_p	K_i	K_d
Conventional	0.8177	0.1893	0.3908	0.8177	0.1893	0.3908	0.8177	0.1893	0.3908
GA	22.2105	67.3446	14.1122	18.79	140.55	23.18	20.9071	33.7624	9.5543
PSO	22.1722	66.9801	14.1081	21.44	60	18.63	22.8070	51.4915	14.4405
ABC	22.1959	62.8050	13.4827	16.907	138.079	20.729	22.1114	65.7727	13.6213
FA	5.8933	8.9221	21.5548	10.014	1.0915	14.715	4.9795	6.4586	2.0571

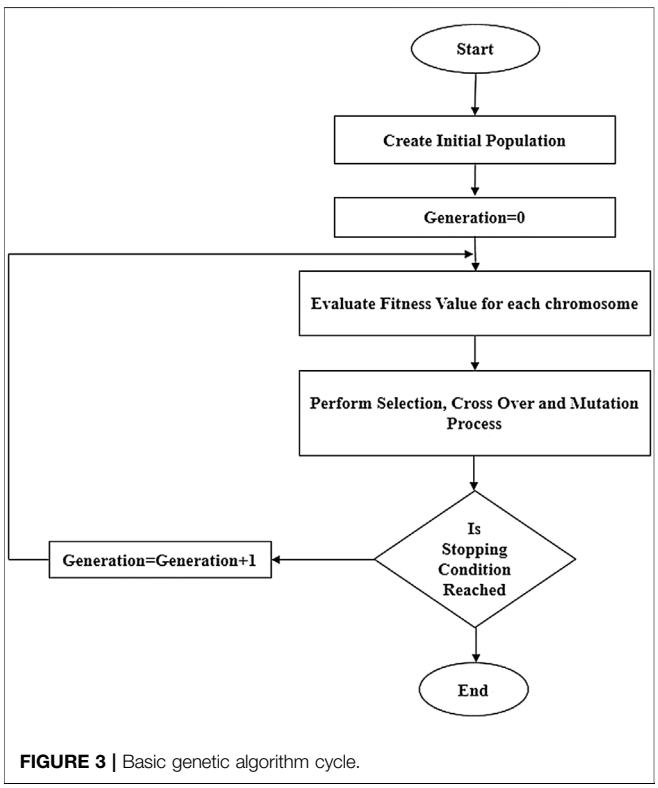

FIGURE 3 | Basic genetic algorithm cycle.

γ is called the coefficient of absorption. It is used to control the flashing light concentration. Fireflies' positions and movement can be described by the following equations.

$$v_i^d(t+1) = rand_i \times v_i^d(t) \times a_i^d(t) \tag{17}$$

$$x_i^d(t) = x_i^d(t) + \beta_0 e^{-\gamma r^2}\left(x_j - x_i\right) + v_i^d(t+1) + \alpha\varepsilon \tag{18}$$

x_i indicates the instantaneous position of the firefly whereas $\alpha\varepsilon$ represents the random behavior of firefly when the firefly can't see another brighter firefly (Naidu et al., 2013; Shakarami et al., 2013; Padhan et al., 2014; Chandra Sekhar et al., 2016; Abd-Elazim and Ali, 2018; Boddepalli and Navuri, 2018; Gupta et al., 2021).

The PID controller proportional gain K_p, integral gain K_i, and derivative gain K_d optimal values have been searched in the range (−10, 150) using firefly algorithm. Firefly algorithm operators used to find out the PID gain values are given in **Table 4** and obtained optimal PID parameters in **Table 5**.

Artificial Bee Colony

Artificial bee colony is meta-heuristic optimization algorithm developed by Karaboğa in 2005. Honey bees foraging behavior has been utilized in this technique searching for nectar at different positions. Usually, three kind of honey bees are considered to be responsible for finding nectar positions: employed, onlooker and scouts. This algorithm adopts some variables and steps to proceed for finding optimal solution. The variables of ABC algorithm include population of honey bees (SN), maximum cycle number (MCN), objective functions and some functions to test the probability, fitness and optimization of the objective functions. The steps in the ABC algorithm includes initialization, employed, onlooker and scout bees. The initialization step starts by generating the number of solutions equal to total number of bees (SN). Each solution is obtained within the upper and lower limit of the selected decision variable with the following equation.

$$x_{ij} = x_j^{min} + rand\ [0,1]\left(x_j^{max} - x_j^{min}\right), i = 1,2,3,\ldots SN, \quad j = 1,2,3,\ldots .D \tag{19}$$

Where D denotes the total number of decision variables used in the objective function. The next step starts by generating the new food source by employed and onlooker bees by updating their positions as given by,

$$v_{ij} = x_{ij} + \varnothing_{ij}\left(x_{ij} - x_{kj}\right), \text{While } i \neq j \tag{20}$$

Where $\varnothing_{ij}$ is random number within range (−1, 1) and used to change the position around x_{ij}. The last step includes the probability of finding the nectar by onlooker bees, which is given by following expression,

$$P_i = \frac{fit_i}{\sum_{n=1}^{Sn} fit_n} \tag{21}$$

Where fit_i is the fitness value corresponding to nectar position i. The fitness value is checked for the next iteration, and if it is better than previous fitness value the latest one is stored and the algorithm continues until the stopping criteria is reached (Ghasemi and Shayeghi, 2011; Rathor et al., 2011; Gozde et al., 2012; Naidu et al., 2014; Elsisi et al., 2015; Kouba et al., 2015; Kumar et al., 2017; Abo-Elyousr, 2018). Using the artificial bee colony, optimized PID controller parameters are found as shown in **Table 5**.

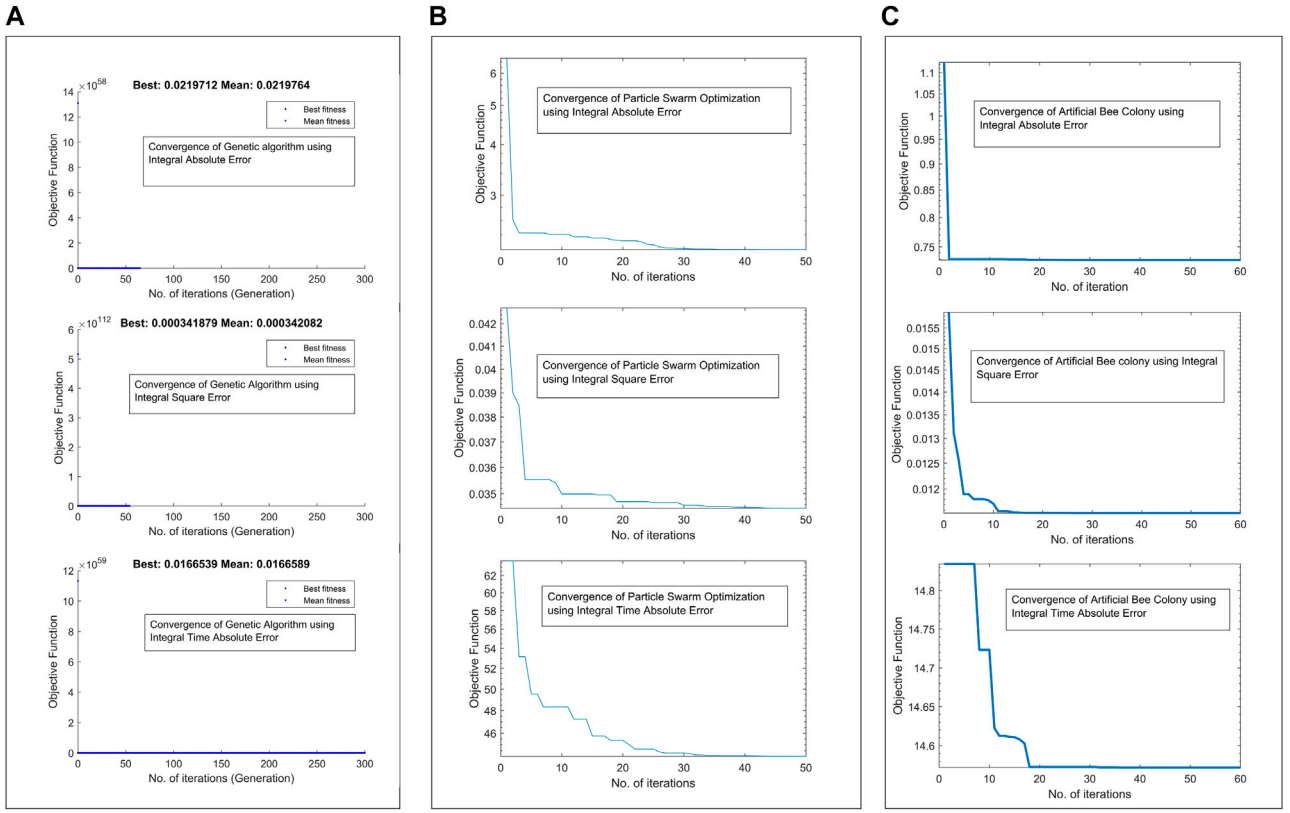

FIGURE 4 | Convergence characteristics of optimization techniques **(A)** GA **(B)** PSO **(C)** ABC.

Conventional PID Controller

The Simulink model of the single-area power system containing PID controller is tuned using the classical method to enhance the performance and robustness. PID Tuner toolbox is launched from the Simulink model that automatically computes the linear power system model to find gain parameters corresponding to initial controller conditions. The obtained PID controller gains can robustly stabilize the power system. The performance of controller could be checked using frequency deviation performance indicators, i.e., settling time, zero steady state error. If the desired response is not achieved by auto tunning, PID controller gains can be adjusted manually by varying the response time (seconds) and transient behavior. The PID controller gains are updated to the Simulink model after meeting the desired requirement (MathWorks, 2022a)- (MathWorks, 2022b). The compensator formula for PID controller is given as,

$$\text{Compensation Formula} = P + I\frac{1}{s} + D\frac{N}{1 + N\frac{1}{s}} \qquad (22)$$

In the studied model, best performing PID controller gains have been found to be K_p 0.8177, K_i 0.1893, and K_d 0.3908 within the range (0, 1) corresponding to initial controller conditions. PID controller has been tuned with response time value of 13.63 s and transient behavior value of 0.6 between aggressiveness and robustness. Filter coefficient N value has been chosen as 100 for this case.

RESULTS AND DISCUSSION

Three objective functions IAE, ISE, and ITAE have been applied to the genetic algorithm, particle swarm optimization, artificial bee colony, and firefly algorithm to find out the optimal proportional gain K_p, integral gain K_i, and derivative gain K_d. **Table 5** illustrates the PID gain parameters for GA, PSO, ABC, and FA using three objective functions. GA, PSO, and ABC techniques have found to be competitive and efficient than FA and conventional methods. The convergence characteristics of GA, PSO, and ABC are shown in **Figure 4**. The graph represents the objective function vs. number of iterations. The graph depicts almost two iterations are required to reach the best fitness 0.0219, 0.00034, and 0.0166 using IAE, ISE, and ITAE objective function respectively for genetic algorithm. It can also be seen that almost 40 iterations are required to reach the best fitness 2.20, 0.0344, and 44.0306 using IAE, ISE, and ITAE cost function respectively for particle swarm optimization. No significant change has been observed after 40 iterations. The fitness value has been found 0.73, 0.0115, and 14.55 using IAE, ISE, and ITAE objective function respectively in less than 20 iterations for artificial bee

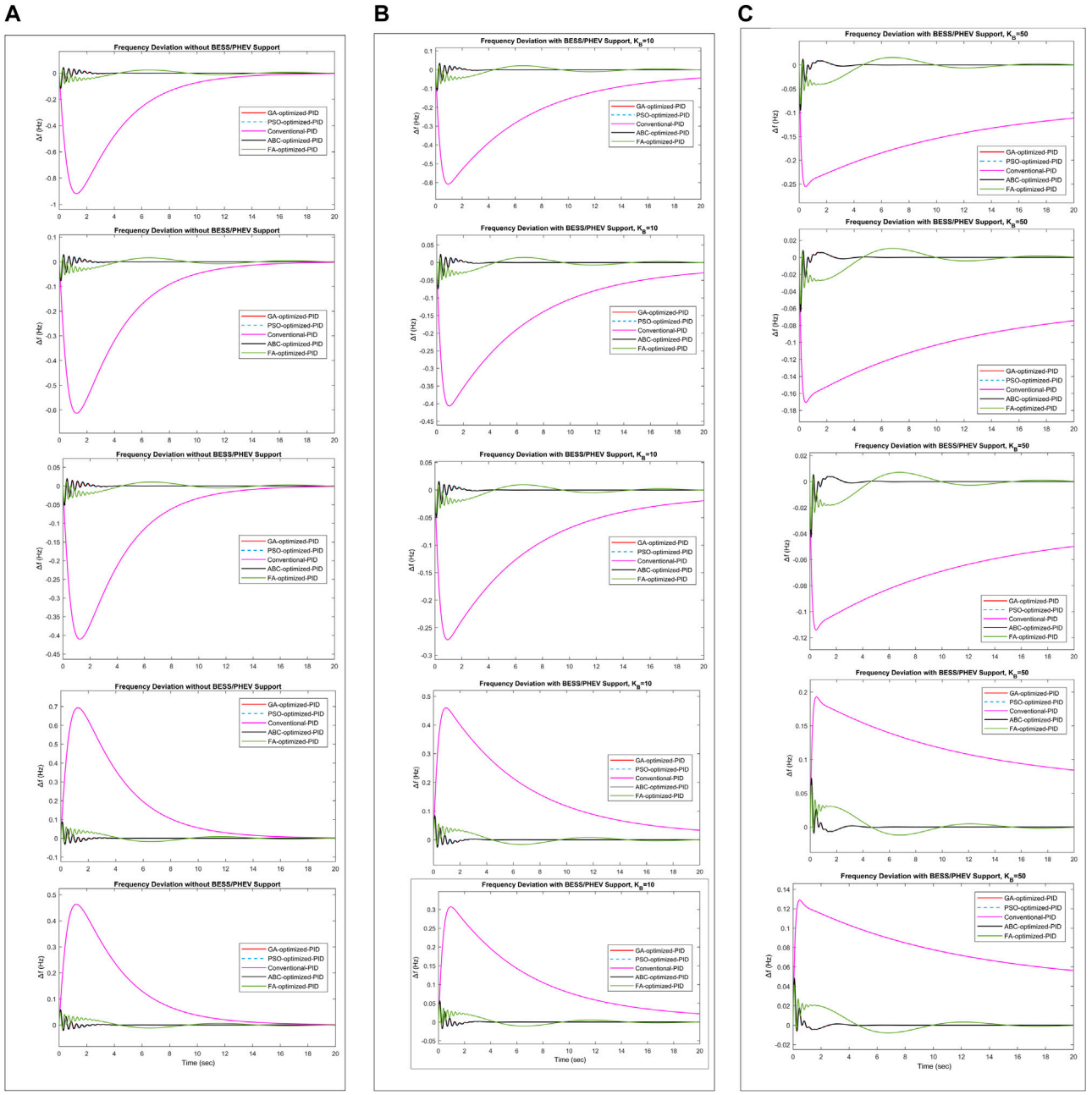

FIGURE 5 | Frequency deviation response using integral absolute error **(A)** without BESS/PHEV support **(B)** with BESS/PHEV support, K_B = 10 **(C)** with BESS/PHEV support, K_B = 50.

colony. Convergence properties describe the effective genetic algorithm that requires very few iterations to reach its best fitness value.

The results of the studied model have been categorized into three cases.

- Frequency damping using integral absolute error (IAE) objective function, with and without BESS/PHEV support.
- Frequency damping using integral square error (ISE) objective function, with and without BESS/PHEV support.
- Frequency damping using integral time absolute error (ITAE) objective function, with and without BESS/PHEV support.

Several parameters are used to check the performance indices of hybrid power system for frequency deviation including integral

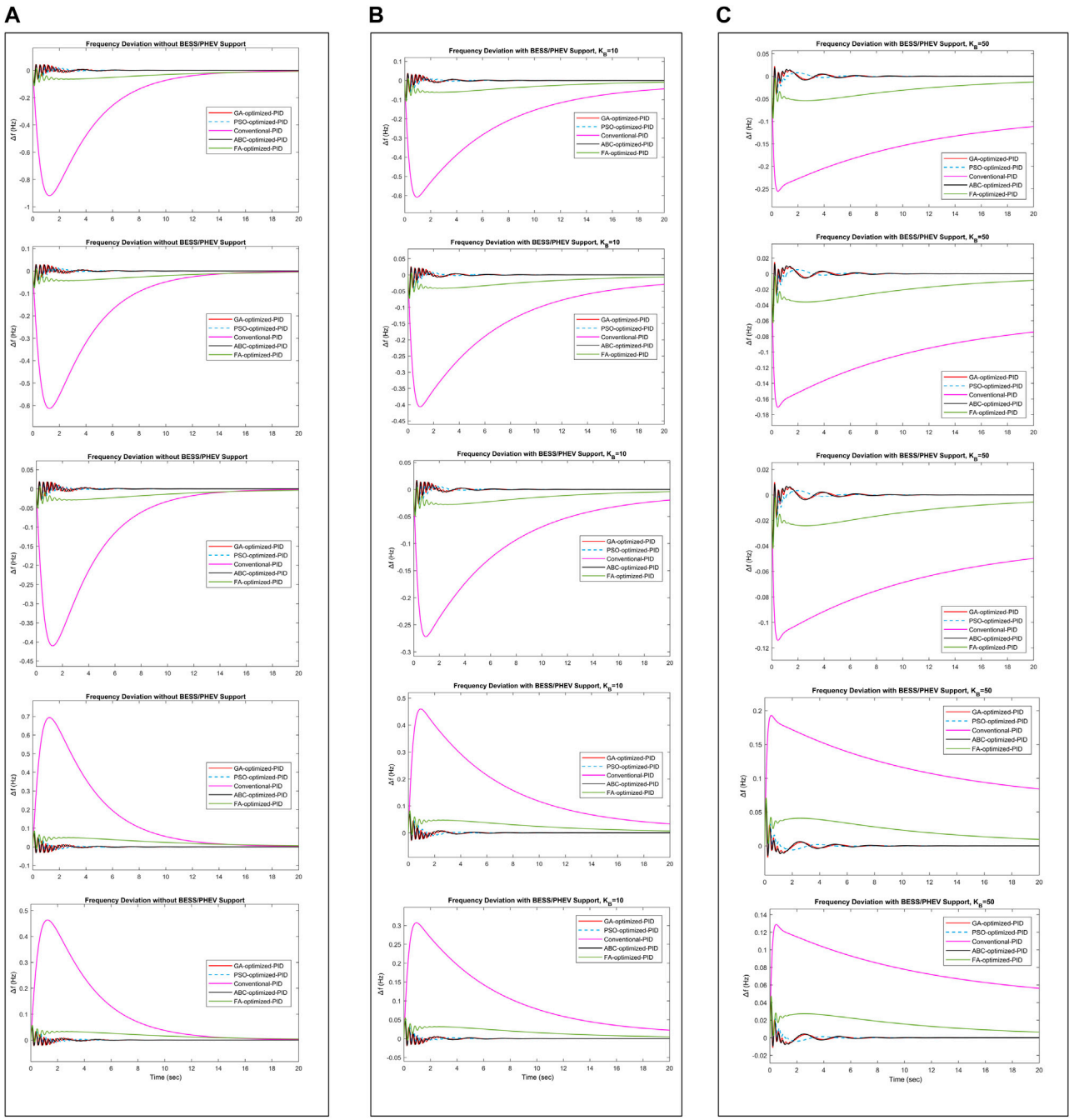

FIGURE 6 | Frequency deviation response using integral square error **(A)** without BESS/PHEV support **(B)** with BESS/PHEV support, K_B = 10 **(C)** with BESS/PHEV support, K_B = 50.

absolute error, integral square error, and integral time absolute error. Rise time $T_r(s)$, settling time $T_s(s)$, peak overshoot $M_P(\%)$, and maximum frequency deviation $\Delta f(Hz)$ are also used to check the transient response of the power system. These performance indices are also checked by integrating power from BESS/PHEV for different capacities to see the frequency deviation suppression.

Frequency of the power system deviates either positive or negative depending upon the increase or decrease in load and photovoltaic power. The mismatch between load demand and photovoltaic power give rise to changes in frequency. Five key days, 1st January (ΔP_L = 0.3394 pu), 30th March (ΔP_L = 0.2374 pu), 13th December (ΔP_L = 0.1575 pu), 24th May (ΔP_L = −0.2275 pu), and 28th

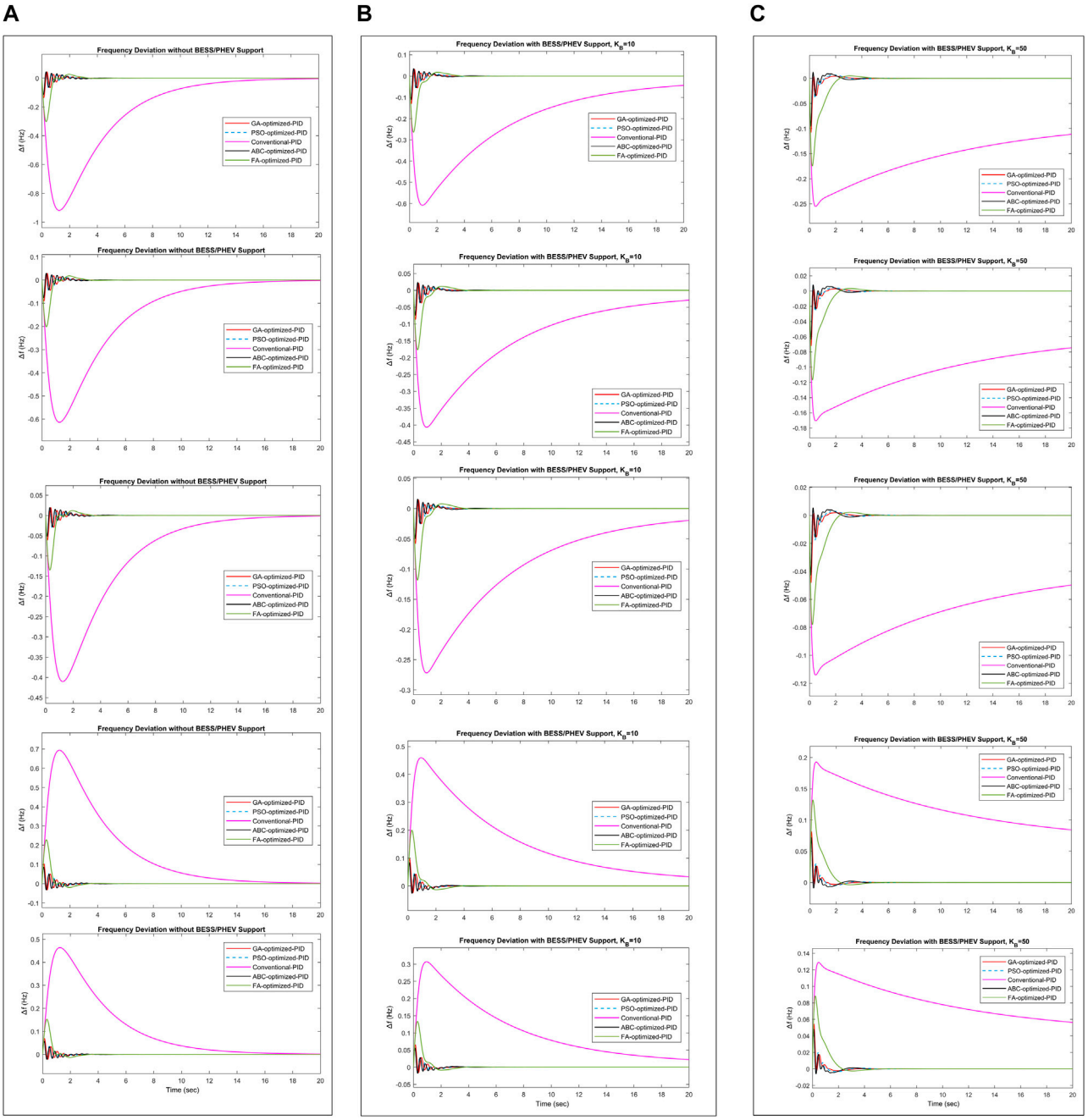

FIGURE 7 | Frequency deviation response using integral time absolute error **(A)** without BESS/PHEV support **(B)** with BESS/PHEV support, K_B = 10 **(C)** with BESS/PHEV support, K_B = 50.

September (ΔP_L = −0.1499 pu), showing significant load changes have been selected to check the conventional PID, GA optimized PID, PSO optimized PID, ABC optimized PID, and FA optimized PID responses against frequency deviation. **Figures 5–7** depicts the frequency deviation responses of the power system in the same order as mentioned above from top to bottom.

Frequency deviation responses of the GA optimized PID, PSO optimized PID, ABC optimized PID, and FA optimized PID using the IAE objective function is shown in **Table 6** and **Figure 5**. Their performance indices show that GA optimized PID, PSO optimized PID, and ABC optimized PID produce approximately same results as their proportional, integral, and derivative values have been found to be same. IAE, ISE, ITAE and

TABLE 6 | Frequency deviation parameter indices using integral absolute error objective function.

Without BESS/PHEV support, K_B = 10 and K_B = 50

Date	ΔP_L	ΔP_{PV}	IAE	ISE	ITAE	T_r (s)	T_s (s)	M_P (%)	Δf (Hz)
Conventional-PID									
1st Jan	0.3394	0.01351	1.718	0.3893	6.502	0.912	7.97	8.15	–0.9184
30th Mar	0.2374	0.01969	1.148	0.1738	4.345	0.912	7.97	8.15	–0.6136
13th Dec	0.1575	0.01192	0.7674	0.07772	2.905	0.912	7.97	8.15	–0.4103
24th May	–0.2275	0.0185	1.297	0.2219	4.909	0.912	7.97	8.15	0.6934
28th Sep	–0.1499	0.01451	0.8666	0.0991	3.281	0.912	7.97	8.15	0.4634
GA-optimized-PID									
1st Jan	0.3394	0.01351	0.02199	0.0003987	0.01991	0.0673	2.87	78.7	–0.1148
30th Mar	0.2374	0.01969	0.01469	0.000178	0.01331	0.0673	2.87	78.7	–0.07668
13th Dec	0.1575	0.01192	0.009823	0.0000795	0.008897	0.0673	2.87	78.7	–0.05132
24th May	–0.2275	0.0185	0.0166	0.0002272	0.01503	0.0673	2.87	78.7	0.08664
28th Sep	–0.1499	0.01451	0.01109	0.0001015	0.01005	0.0673	2.87	78.7	0.05792
PSO-optimized-PID									
1st Jan	0.3394	0.01351	0.02199	0.0003987	0.01994	0.0673	2.86	78.6	–0.1148
30th Mar	0.2374	0.01969	0.01469	0.000178	0.01332	0.0673	2.86	78.6	–0.07668
13th Dec	0.1575	0.01192	0.009824	0.0000795	0.00891	0.0673	2.86	78.6	–0.05132
24th May	–0.2275	0.0185	0.0166	0.0002272	0.01506	0.0673	2.86	78.6	0.08664
28th Sep	–0.1499	0.01451	0.01109	0.0001015	0.01006	0.0673	2.86	78.6	0.05792
ABC-optimized-PID									
1st Jan	0.3394	0.01351	0.022	0.0004133	0.01913	0.069	2.77	78	–0.1171
30th Mar	0.2374	0.01969	0.0147	0.000184	0.01278	0.069	2.77	78	–0.0783
13th Dec	0.1575	0.01192	0.009831	0.000082	0.00854	0.069	2.77	78	–0.0523
24th May	–0.2275	0.0185	0.01661	0.000235	0.01444	0.069	2.77	78	0.0885
28th Sep	–0.1499	0.01451	0.0111	0.000105	0.00965	0.069	2.77	78	0.05918
FA-optimized-PID									
1st Jan	0.3394	0.01351	0.1106	0.001322	0.61	0.0548	3.84	76.9	–0.09573
30th Mar	0.2374	0.01969	0.0739	0.00059	0.4076	0.0548	3.84	76.9	–0.0641
13th Dec	0.1575	0.01192	0.0493	0.000264	0.2725	0.0548	3.84	76.9	–0.0428
24th May	–0.2275	0.0185	0.08352	0.000753	0.4605	0.0548	3.84	76.9	0.0722
28th Sep	–0.1499	0.01451	0.05882	0.000336	0.3078	0.0548	3.84	76.9	0.0484

With BESS/PHEV support, K_B = 10 **and** K_B = 50

Date	ΔP_L	ΔP_{PV}	IAE		ISE		ITAE		T_r (s)		T_s (s)		M_P (%)		Δf (Hz)	
			K_B = 10	K_B = 50	K_B = 10	K_B = 50	K_B = 10	K_B = 50	K_B = 10	K_B = 50	K_B = 10	K_B = 50	K_B = 10	K_B = 50	K_B = 10	K_B = 50
Conventional-PID																
1st Jan	0.3394	0.01351	1.72	1.299	0.2356	0.08956	10.24	11.27	7.93	—	693	—	10.1	—	–0.6085	–0.2554
30th Mar	0.2374	0.01969	1.149	0.8681	0.1052	0.03998	6.839	7.53	7.93	—	693	—	10.1	—	–0.4066	–0.1705
13th Dec	0.1575	0.01192	0.7885	0.5805	0.04703	0.01788	4.573	5.035	7.93	—	693	—	10.1	—	–0.2719	–0.1140

(Continued on following page)

TABLE 6 | (*Continued*) Frequency deviation parameter indices using integral absolute error objective function.

Without BESS/PHEV support, K_B = 10 and K_B = 50																
Date	**ΔP_L**	**ΔP_{PV}**	**IAE**		**ISE**		**ITAE**		**T_r (s)**		**T_s (s)**		**M_P (%)**		**Δf (Hz)**	
24th May	−0.2275	0.0185	1.299	0.9809	0.1343	0.05105	7.728	8.509	7.93	—	693	—	10.1	—	0.4594	0.1928
28th Sep	−0.1499	0.01451	0.8678	0.6555	0.05997	0.0228	5.164	5.686	7.93	—	693	—	10.1	—	0.3070	0.1289
GA-Optimized-PID																
1st Jan	0.3394	0.01351	0.01873	0.01353	0.0003203	0.0001902	0.01696	0.01399	0.0683	0.0738	2.3	1.75	70	41	−0.1103	−0.09469
30th Mar	0.2374	0.01969	0.01252	0.00904	0.000143	0.0000848	0.01133	0.009344	0.0683	0.0738	2.3	1.75	70	41	−0.07368	−0.06326
13th Dec	0.1575	0.01192	0.00837	0.006045	0.0000639	0.0000379	0.007576	0.006248	0.0683	0.0738	2.3	1.75	70	41	−0.04928	−0.04229
24th May	−0.2275	0.0185	0.01414	0.01022	0.0001826	0.0001083	0.0128	0.01056	0.0683	0.0738	2.3	1.75	70	41	0.08323	0.07146
28th Sep	−0.1499	0.01451	0.009452	0.006827	0.0000815	0.0000483	0.008555	0.007056	0.0683	0.0738	2.3	1.75	70	41	0.05561	0.04779
PSO-Optimized-PID																
1st Jan	0.3394	0.01351	0.01874	0.01355	0.0003205	0.0001902	0.01699	0.01402	0.0683	0.0738	2.3	1.75	69.9	40.9	−0.1103	−0.09469
30th Mar	0.2374	0.01969	0.01252	0.009052	0.0001431	0.0000849	0.01135	0.00937	0.0683	0.0738	2.3	1.75	69.9	40.9	−0.07368	−0.06326
13th Dec	0.1575	0.01192	0.008373	0.006053	0.0000639	0.0000379	0.007589	0.006265	0.0683	0.0738	2.3	1.75	69.9	40.9	−0.04928	−0.04229
24th May	−0.2275	0.0185	0.01415	0.01023	0.0001827	0.0001084	0.01282	0.01059	0.0683	0.0738	2.3	1.75	69.9	40.9	0.08323	0.07146
28th Sep	−0.1499	0.01451	0.009455	0.006835	0.0000815	0.0000484	0.00857	0.007075	0.0683	0.0738	2.3	1.75	69.9	40.9	0.05561	0.04779
ABC-optimized-PID																
1st Jan	0.3394	0.01351	0.01872	0.01346	0.0003236	0.000197	0.01619	0.01324	0.07	0.0756	2.3	1.77	69.1	40	−0.1122	−0.0959
30th Mar	0.2374	0.01969	0.01251	0.00899	0.0001485	0.000088	0.01082	0.00884	0.07	0.0756	2.3	1.77	69.1	40	−0.0749	−0.064
13th Dec	0.1575	0.01192	0.00836	0.00611	0.0000664	0.000039	0.00723	0.00591	0.07	0.0756	2.3	1.77	69.1	40	−0.0501	−0.0429
24th May	−0.2275	0.0185	0.01413	0.01017	0.000189	0.000112	0.01222	0.00999	0.07	0.0756	2.3	1.77	69.1	40	0.0847	0.0724
28th Sep	−0.1499	0.01451	0.00944	0.00679	0.000084	0.000050	0.008168	0.00667	0.07	0.0756	2.3	1.77	69.1	40	0.0566	0.0484
FA-optimized-PID																
1st Jan	0.3394	0.01351	0.1041	0.0844	0.001192	0.00087	0.5558	0.399	0.0553	0.059	2.75	8.98	69.9	46.1	−0.0926	−0.0823
30th Mar	0.2374	0.01969	0.0695	0.05642	0.000532	0.000388	0.3714	0.266	0.0553	0.059	2.75	8.98	69.9	46.1	−0.0619	0.05504
13th Dec	0.1575	0.01192	0.0465	0.0377	0.000237	0.000173	0.2483	0.1782	0.0553	0.059	2.75	8.98	69.9	46.1	−0.0414	−0.0366
24th May	−0.2275	0.0185	0.0786	0.0637	0.000679	0.000496	0.4196	0.3012	0.0553	0.059	2.75	8.98	69.9	46.1	0.070	0.06194
28th Sep	−0.1499	0.01451	0.05254	0.0426	0.000303	0.000221	0.2804	0.2013	0.0553	0.059	2.75	8.98	69.9	46.1	0.0468	0.0415

TABLE 7 | Frequency deviation parameter indices using integral square error objective function.

Without BESS/PHEV support

Date	ΔP_L	ΔP_{PV}	IAE	ISE	ITAE	T_r (s)	T_s (s)	M_P (%)	Δf (Hz)
Conventional-PID									
1st Jan	0.3394	0.01351	1.718	0.3893	6.502	0.912	7.97	8.15	−0.9184
30th Mar	0.2374	0.01969	1.148	0.1738	4.345	0.912	7.97	8.15	−0.6136
13th Dec	0.1575	0.01192	0.7674	0.07772	2.905	0.912	7.97	8.15	−0.4103
24th May	−0.2275	0.0185	1.297	0.2219	4.909	0.912	7.97	8.15	0.6934
28th Sep	−0.1499	0.01451	0.8666	0.0991	3.281	0.912	7.97	8.15	0.4634
GA-Optimized-PID									
1st Jan	0.3394	0.01351	0.02719	0.0003375	0.04641	0.0518	4.51	87	−0.09178
30th Mar	0.2374	0.01969	0.01817	0.0001507	0.03101	0.0518	4.51	87	−0.06102
13th Dec	0.1575	0.01192	0.01215	0.0000673	0.02074	0.0518	4.51	87	−0.04110
24th May	−0.2275	0.0185	0.02053	0.0001924	0.03504	0.0518	4.51	87	0.06937
28th Sep	−0.1499	0.01451	0.01372	0.0000859	0.02342	0.0518	4.51	87	0.04637
PSO-Optimized-PID									
1st Jan	0.3394	0.01351	0.02339	0.0003489	0.02866	0.0581	3.35	81.6	−0.1014
30th Mar	0.2374	0.01969	0.01563	0.0001557	0.01915	0.0581	3.35	81.6	−0.06781
13th Dec	0.1575	0.01192	0.01045	0.00006964	0.0128	0.0581	3.35	81.6	−0.04532
24th May	−0.2275	0.0185	0.01766	0.0001988	0.02164	0.0581	3.35	81.6	0.0766
28th Sep	−0.1499	0.01451	0.0118	0.0000888	0.01446	0.0581	3.35	81.6	0.05118
ABC-optimized-PID									
1st Jan	0.3394	0.01351	0.02629	0.000327	0.04707	0.0551	3.37	84	−0.0966
30th Mar	0.2374	0.01969	0.01758	0.000146	0.03145	0.0551	3.37	84	−0.0644
13th Dec	0.1575	0.01192	0.01174	0.000065	0.02103	0.0551	3.37	84	−0.0431
24th May	−0.2275	0.0185	0.01985	0.0001868	0.03554	0.0551	3.37	84	0.0731
28th Sep	−0.1499	0.01451	0.01326	0.0000834	0.02375	0.0551	3.37	84	0.0487
FA-optimized-PID									
1st Jan	0.3394	0.01351	0.2756	0.005127	1.896	0.0677	2.27	67.9	−0.1146
30th Mar	0.2374	0.01969	0.1841	0.00228	1.267	0.0677	2.27	67.9	−0.0764
13th Dec	0.1575	0.01192	0.1231	0.00102	0.8469	0.0677	2.27	67.9	−0.0511
24th May	−0.2275	0.0185	0.2081	0.002922	1.432	0.0677	2.27	67.9	0.0865
28th Sep	−0.1499	0.01451	0.139	0.001305	0.9564	0.0677	2.27	67.9	0.0577

With BESS/PHEV support, K_B = 10 and K_B = 50

Date	ΔP_L	ΔP_{PV}	IAE		ISE		ITAE		T_r (s)		T_s (s)		M_P (%)		Δf (Hz)	
			K_B = 10	K_B = 50	K_B = 10	K_B = 50	K_B = 10	K_B = 50	K_B = 10	K_B = 50	K_B = 10	K_B = 50	K_B = 10	K_B = 50	K_B = 10	K_B = 50
Conventional-PID																
1st Jan	0.3394	0.01351	1.72	1.299	0.2356	0.08956	10.24	11.27	7.93	—	693	—	10.1	—	−0.6085	−0.2554
30th Mar	0.2374	0.01969	1.149	0.8681	0.1052	0.03998	6.839	7.53	7.93	—	693	—	10.1	—	−0.4066	−0.1705

(Continued on following page)

TABLE 7 | (*Continued*) Frequency deviation parameter indices using integral square error objective function.

With BESS/PHEV support, K_B = 10 and K_B = 50																
Date	**ΔP_L**	**ΔP_{PV}**	**IAE**		**ISE**		**ITAE**		**T_r (s)**		**T_s (s)**		**M_P (%)**		**Δf (Hz)**	
13th Dec	0.1575	0.01192	0.7885	0.5805	0.04703	0.01788	4.573	5.035	7.93	—	693	—	10.1	—	−0.2719	−0.1140
24th May	−0.2275	0.0185	1.299	0.9809	0.1343	0.05105	7.728	8.509	7.93	—	693	—	10.1	—	0.4594	0.1928
28th Sep	−0.1499	0.01451	0.8678	0.6555	0.05997	0.0228	5.164	5.686	7.93	—	693	—	10.1	—	0.3070	0.1289
GA-optimized-PID																
1st Jan	0.3394	0.01351	0.02258	0.01686	0.0002532	0.0001398	0.03997	0.03458	0.0522	0.0551	3.42	2.77	80	55.9	−0.08901	−0.07942
30th Mar	0.2374	0.01969	0.01509	0.01126	0.000113	0.0000624	0.02871	0.02311	0.0522	0.0551	3.42	2.77	80	55.9	−0.05950	−0.05293
13th Dec	0.1575	0.01192	0.01009	0.007531	0.0000505	0.0000279	0.01788	0.01545	0.0522	0.0551	3.42	2.77	80	55.9	−0.03987	−0.03547
24th May	−0.2275	0.0185	0.01705	0.01273	0.0001443	0.0000796	0.03018	0.02611	0.0522	0.0551	3.42	2.77	80	55.9	0.06738	0.05988
28th Sep	−0.1499	0.01451	0.01139	0.008505	0.0000644	0.0000355	0.02017	0.01745	0.0522	0.0551	3.42	2.77	80	55.9	0.04506	0.04005
PSO-optimized-PID																
1st Jan	0.3394	0.01351	0.01997	0.01475	0.0002766	0.0001646	0.02497	0.02049	0.0588	0.0628	2.64	2.2	74	47.8	−0.09794	−0.08589
30th Mar	0.2374	0.01969	0.01334	0.009856	0.0001235	0.00007347	0.01668	0.01369	0.0588	0.0628	2.64	2.2	74	47.8	−0.06544	−0.05740
13th Dec	0.1575	0.01192	0.00892	0.00659	0.0000552	0.00003285	0.01116	0.00915	0.0588	0.0628	2.64	2.2	74	47.8	−0.04378	−0.03838
24th May	−0.2275	0.0185	0.01508	0.01114	0.0001577	0.0000938	0.01885	0.0154	0.0588	0.0628	2.64	2.2	74	47.8	0.07401	0.06494
28th Sep	−0.1499	0.01451	0.01008	0.007442	0.0000704	0.0000419	0.0126	0.01034	0.0588	0.0628	2.64	2.2	74	47.8	0.04944	0.04341
ABC-optimized-PID																
1st Jan	0.3394	0.01351	0.02323	0.01835	0.00026	0.000155	0.0437	0.03927	0.055	0.059	2.9	2.7	76.7	51.6	−0.09344	−0.08275
30th Mar	0.2374	0.01969	0.01552	0.01226	0.00011	0.000069	0.0292	0.02624	0.055	0.059	2.9	2.7	76.7	51.6	−0.0624	−0.0554
13th Dec	0.1575	0.01192	0.01038	0.00819	0.000519	0.000031	0.0195	0.01755	0.055	0.059	2.9	2.7	76.7	51.6	−0.041	−0.037
24th May	−0.2275	0.0185	0.01754	0.01385	0.000148	0.000088	0.03299	0.02965	0.055	0.059	2.9	2.7	76.7	51.6	0.0706	0.0625
28th Sep	−0.1499	0.01451	0.01172	0.009257	0.000066	0.000039	0.02205	0.01981	0.055	0.059	2.9	2.7	76.7	51.6	0.0471	0.0417
FA-optimized-PID																
1st Jan	0.3394	0.01351	0.2726	0.2601	0.00486	0.00405	1.925	1.986	0.0686	8.24	8.47	488	59.8	7.85	−0.1098	−0.09428
30th Mar	0.2374	0.01969	0.1821	0.1738	0.00217	0.00181	1.286	1.327	0.0686	8.24	8.47	488	59.8	7.85	−0.0733	−0.0629
13th Dec	0.1575	0.01192	0.1218	0.1162	0.00097	0.00081	0.86	0.8872	0.0686	8.24	8.47	488	59.8	7.85	−0.049	−0.042
24th May	−0.2275	0.0185	0.2058	0.1964	0.00277	0.0023	1.453	1.499	0.0686	8.24	8.47	488	59.8	7.85	0.0828	0.0712
28th Sep	−0.1499	0.01451	0.1375	0.1312	0.001237	0.00103	0.9711	1.002	0.0686	8.24	8.47	488	59.8	7.85	0.0554	0.0476

TABLE 8 | Frequency deviation parameter indices using integral time absolute error objective function.

Without BESS/PHEV support

Date	ΔP_L	ΔP_{PV}	IAE	ISE	ITAE	T_r (s)	T_s (s)	M_P (%)	Δf (Hz)
Conventional-PID									
1st Jan	0.3394	0.01351	1.718	0.3893	6.502	0.912	7.97	8.15	–0.9184
30th Mar	0.2374	0.01969	1.148	0.1738	4.345	0.912	7.97	8.15	–0.6136
13th Dec	0.1575	0.01192	0.7674	0.07772	2.905	0.912	7.97	8.15	–0.4103
24th May	–0.2275	0.0185	1.297	0.2219	4.909	0.912	7.97	8.15	0.6934
28th Sep	–0.1499	0.01451	0.8666	0.0991	3.281	0.912	7.97	8.15	0.4634
GA-optimized-PID									
1st Jan	0.3394	0.01351	0.02375	0.0005794	0.01643	0.0827	2.55	73.4	–0.1374
30th Mar	0.2374	0.01969	0.01587	0.0002587	0.01098	0.0827	2.55	73.4	–0.09176
13th Dec	0.1575	0.01192	0.01061	0.0001157	0.007339	0.0827	2.55	73.4	–0.06134
24th May	–0.2275	0.0185	0.01793	0.0003302	0.0124	0.0827	2.55	73.4	0.1037
28th Sep	–0.1499	0.01451	0.01198	0.0001475	0.008287	0.0827	2.55	73.4	0.06925
PSO-optimized-PID									
1st Jan	0.3394	0.01351	0.02201	0.0003988	0.01991	0.0665	3.03	78.4	–0.1136
30th Mar	0.2374	0.01969	0.0147	0.000178	0.0133	0.0665	3.03	78.4	–0.07594
13th Dec	0.1575	0.01192	0.009388	0.0000725	0.008493	0.0665	3.03	78.4	–0.04849
24th May	–0.2275	0.0185	0.01662	0.0002273	0.01503	0.0665	3.03	78.4	0.08579
28th Sep	–0.1499	0.01451	0.0111	0.0001015	0.01004	0.0665	3.03	78.4	0.05736
ABC-optimized-PID									
1st Jan	0.3394	0.01351	0.022	0.000409	0.01936	0.0686	2.76	78.2	–0.1165
30th Mar	0.2374	0.01969	0.0147	0.0001827	0.01293	0.0686	2.76	78.2	–0.0778
13th Dec	0.1575	0.01192	0.00982	0.0000817	0.00864	0.0686	2.76	78.2	–0.052
24th May	–0.2275	0.0185	0.01661	0.000233	0.01462	0.0686	2.76	78.2	0.088
28th Sep	–0.1499	0.01451	0.0111	0.000104	0.00976	0.0686	2.76	78.2	0.0588
FA-optimized-PID									
1st Jan	0.3394	0.01351	0.07121	0.005468	0.04984	0.205	1.84	45.5	–0.3024
30th Mar	0.2374	0.01969	0.04758	0.002441	0.0333	0.205	1.84	45.5	–0.202
13th Dec	0.1575	0.01192	0.03182	0.00109	0.0222	0.205	1.84	45.5	–0.135
24th May	–0.2275	0.0185	0.05376	0.003117	0.03763	0.205	1.84	45.5	0.228
28th Sep	–0.1499	0.01451	0.03593	0.00139	0.02515	0.205	1.84	45.5	0.1526

With BESS/PHEV support, K_B = 10 and K_B = 50

Date	ΔP_L	ΔP_{PV}	IAE		ISE		ITAE		T_r (s)		T_s (s)		M_P (%)		Δf (Hz)	
			K_B = 10	K_B = 50	K_B = 10	K_B = 50	K_B = 10	K_B = 50	K_B = 10	K_B = 50	K_B = 10	K_B = 50	K_B = 10	K_B = 50	K_B = 10	K_B = 50
Conventional-PID																
1st Jan	0.3394	0.01351	1.72	1.299	0.2356	0.08956	10.24	11.27	7.93	—	693	—	10.1	—	–0.6085	–0.2554
30th Mar	0.2374	0.01969	1.149	0.8681	0.1052	0.03998	6.839	7.53	7.93	—	693	—	10.1	—	–0.4066	–0.1705
13th Dec	0.1575	0.01192	0.7885	0.5805	0.04703	0.01788	4.573	5.035	7.93	—	693	—	10.1	—	–0.2719	–0.1140

(Continued on following page)

TABLE 8 | (*Continued*) Frequency deviation parameter indices using integral time absolute error objective function.

With BESS/PHEV support, K_B = 10 and K_B = 50																
Date	**ΔP_L**	**ΔP_{PV}**	**IAE**		**ISE**		**ITAE**		**T_r (s)**		**T_s (s)**		**M_P (%)**		**Δf (Hz)**	
			K_B = 10	**K_B = 50**	**K_B = 10**	**K_B = 50**	**K_B = 10**	**K_B = 50**	**K_B = 10**	**K_B = 50**	**K_B = 10**	**K_B = 50**	**K_B = 10**	**K_B = 50**	**K_B = 10**	**K_B = 50**
24th May	−0.2275	0.0185	1.299	0.9809	0.1343	0.05105	7.728	8.509	7.93	—	693	—	10.1	—	0.4594	0.1928
28th Sep	−0.1499	0.01451	0.8678	0.6555	0.05997	0.0228	5.164	5.686	7.93	—	693	—	10.1	—	0.3070	0.1289
GA-optimized-PID																
1st Jan	0.3394	0.01351	0.01968	0.01412	0.0004687	0.0002801	0.01284	0.009743	0.0844	0.095	2.04	0.94	63.1	29.9	−0.1302	−0.1080
30th Mar	0.2374	0.01969	0.01315	0.009436	0.0002092	0.000125	0.008581	0.00651	0.0844	0.095	2.04	0.94	63.1	29.9	−0.08699	−0.07205
13th Dec	0.1575	0.01192	0.008793	0.006309	0.0000935	0.0000559	0.005738	0.004353	0.0844	0.095	2.04	0.94	63.1	29.9	−0.05821	−0.04821
24th May	−0.2275	0.0185	0.01486	0.01066	0.0002672	0.0001596	0.009696	0.007356	0.0844	0.095	2.04	0.94	63.1	29.9	0.09831	0.08150
28th Sep	−0.1499	0.01451	0.009929	0.007125	0.0001193	0.0000712	0.006479	0.004915	0.0844	0.095	2.04	0.94	63.1	29.9	0.06569	0.0544
PSO-optimized-PID																
1st Jan	0.3394	0.01351	0.01863	0.01347	0.0003207	0.0001919	0.01673	0.01334	0.0647	0.072	2.25	1.97	69.8	41.4	−0.1092	−0.09385
30th Mar	0.2374	0.01969	0.01245	0.009003	0.0001432	0.0000856	0.01118	0.008912	0.0647	0.072	2.25	1.97	69.8	41.4	−0.07292	−0.06276
13th Dec	0.1575	0.01192	0.007947	0.005748	0.0000583	0.0000349	0.007138	0.00569	0.0647	0.072	2.25	1.97	69.8	41.4	−0.04656	−0.04008
24th May	−0.2275	0.0185	0.01406	0.01017	0.0001828	0.0001094	0.01263	0.01007	0.0647	0.072	2.25	1.97	69.8	41.4	0.08240	0.07091
28th Sep	−0.1499	0.01451	0.009399	0.006798	0.0000816	0.0000488	0.008442	0.00673	0.0647	0.072	2.25	1.97	69.8	41.4	0.05507	0.04742
ABC-optimized-PID																
1st Jan	0.3394	0.01351	0.01877	0.01352	0.000329	0.0001955	0.01653	0.01357	0.0696	0.075	2.3	1.75	69.4	40.3	−0.116	−0.095
30th Mar	0.2374	0.01969	0.01254	0.009035	0.000147	0.000087	0.01104	0.009065	0.0696	0.075	2.3	1.75	69.4	40.3	−0.074	−0.064
13th Dec	0.1575	0.01192	0.00838	0.00604	0.000065	0.000039	0.00738	0.00606	0.0696	0.075	2.3	1.75	69.4	40.3	−0.0499	−0.0427
24th May	−0.2275	0.0185	0.01417	0.01021	0.0001878	0.000111	0.01248	0.01024	0.0696	0.075	2.3	1.75	69.4	40.3	0.0843	0.0722
28th Sep	−0.1499	0.01451	0.00947	0.00682	0.000083	0.000049	0.00833	0.006845	0.0696	0.075	2.3	1.75	69.4	40.3	0.0564	0.04823
FA-optimized-PID																
1st Jan	0.3394	0.01351	0.06825	0.0575	0.00425	0.00220	0.05132	0.05132	0.227	1.12	1.89	1.79	25.6	1.8	−0.264	−0.175
30th Mar	0.2374	0.01969	0.0456	0.03842	0.001897	0.000985	0.03429	0.03429	0.227	1.12	1.89	1.79	25.6	1.8	−0.176	−0.1169
13th Dec	0.1575	0.01192	0.0304	0.02569	0.000848	0.00044	0.0229	0.02293	0.227	1.12	1.89	1.79	25.6	1.8	−0.118	−0.0781
24th May	−0.2275	0.0185	0.0515	0.04341	0.00242	0.001259	0.03875	0.03874	0.227	1.12	1.89	1.79	25.6	1.8	0.2	0.132
28th Sep	−0.1499	0.01451	0.03443	0.02901	0.00108	0.000562	0.02589	0.02589	0.227	1.12	1.89	1.79	25.6	1.8	0.133	0.0882

Δf are higher for higher mismatches between load and photovoltaic generated power and lower for lower mismatches, i.e., The values of IAE, ISE, ISE and Δf are 0.02199, 0.0003987, 0.01991, and −0.1148 for GA, PSO, and ABC considering the 0.3394 pu load deviation and 0.01351 pu solar PV power for 1st January loading situation in single-area power system. These values of IAE, ISE, ITAE and Δf are lowered to 0.01469, 0.000178, 0.01331, and −0.07668 for GA, PSO, and ABC for 0.2374 pu load deviation and 0.0147 pu solar PV power on 13th December loading conditions. FA optimized PID produces relatively poor result as the IAE, ISE, and ITAE values 0.1106, 0.001322, 0.61 for 1st January loading conditions indicate much higher than GA, PSO and ABC. The values of rise time $T_r(s)$, settling $T_s(s)$, and peak overshoot $M_P(\%)$ are same for all loading conditions. For example, the values of $T_r(s)$, settling $T_s(s)$, and peak overshoot $M_P(\%)$ are 0.0673, 2.87, and 78.7 for GA and PSO, 0.069, 2.77, and 78 for ABC on 1st January.

Considering the effect of BESS/PHEV with its different capacities, BESS/PHEV K_B of 10 and 50 are used to check frequency deviation response. Results indicate that settling $T_s(s)$, peak overshoot $M_P(\%)$ are reduced to 2.3, 70 for GA, PSO, and ABC for K_B of 10. These values are further reduced to 1.75 and 40 for K_B of 50. The values of IAE, ISE, ISE and Δf are reduced to 0.01873, 0.0003203, 0.01696, and −0.1103 for GA, PSO, ABC for K_B of 10, and 0.01353, 0.0001902, 0.01399, and −0.0946 for K_B 50 for 1st January loading conditions. Rise time $T_r(s)$ remains unchanged in any case.

Frequency deviation responses of the GA optimized PID, PSO optimized PID, ABC optimized PID, and FA optimized PID using the ISE objective function is shown in **Table 7** and **Figure 6**. Their performance indices show that GA optimized PID, PSO optimized PID, and ABC optimized PID produce efficient and competitive results. IAE, ISE, ITAE and Δf are higher for higher mismatches between load and photovoltaic generated power and lower for lower mismatches, i.e., The values of IAE, ISE, ISE and Δf are 0.02719, 0.0003375, 0.04641, and −0.09178 for GA, 0.02339, 0.0003489, 0.02866, and −0.1014 for PSO, 0.02629, 0.000327, 0.04707, and −0.0966 for ABC considering the 0.3394 pu load deviation and 0.01351 pu solar PV power on 1st January in a single-area power system. These values of IAE, ISE, ITAE and Δf are lowered to 0.01817, 0.0001507, 0.03101, and −0.06102 for GA, 0.01563, 0.0001557, 0.01915, and −0.06781 for PSO, 0.01758, 0.000146, 0.03145 and −0.0644 for ABC for 0.2374 pu load deviation and 0.0147 pu solar PV power on 13th December loading conditions. The values of rise time $T_r(s)$, settling $T_s(s)$, and peak overshoot $M_P(\%)$ remain same for different loading conditions. For example, the values of rise time $T_r(s)$, settling $T_s(s)$, and peak overshoot $M_P(\%)$ are 0.0518, 4.51, and 87 for GA, 0.0581, 3.35, and 81.6 for PSO, 0.0551, 3.37, and 84 for ABC on 1st January loading conditions. FA optimized PID produces relatively poor result as the IAE, ISE, and ITAE values are much higher than GA, PSO and ABC as can be seen their values are 0.275, 0.005127, and 1.896.

Considering the effect of BESS/PHEV with its different capacities, gain for K_B 0f 10 and 50 are taken to check the stability of power system. Results indicate that settling time $T_s(s)$, peak overshoot $M_P(\%)$ are reduced to 3.4, 80 for GA, 2.64, 74 for PSO, and 2.9, 76.7 for ABC for K_B of 10. These values are further reduced to 2.77, 55.9 for GA, 2.2, 47.8 for PSO, and 2.7, 51.6 for ABC for K_B of 50. Similarly, the values of IAE, ISE, ITAE and Δf are reduced to 0.02258, 0.0002532, 0.03997, and −0.08901 for GA, 0.01997, 0.0002766, 0.02497, and −0.09794 for PSO, 0.02323, 0.00026, 0.0437, −0.09344 for ABC, for K_B of 10, and further reduced to 0.01686, 0.0001398, 0.03458, and −0.07942 for GA, 0.01475, 0.0001646, 0.02049, and −0.085859 for PSO, 0.01835, 0.000155, 0.03927, and −0.08275 for ABC, for K_B of 50 for 1st January loading conditions. Rise time $T_r(s)$ remains almost unchanged in any case. FA optimized PID produces high error values although it is connected to BESS/PHEV support. Instead, the settling time reached to 488 s when BESS/PHEV gain is 50. It is concluded that GA optimized PID produces comparatively better result that PSO, ABC, and FA when ISE cost function is used for the load frequency control.

Frequency deviation responses of the GA optimized PID, PSO optimized PID, ABC optimized PID, and FA optimized PID using the ITAE objective function is shown in **Table 8** and **Figure 7**. Their performance indices show that GA optimized PID, PSO optimized PID, and ABC optimized PID produce approximately efficient competitive results. IAE, ISE, ITAE and Δf are higher for higher mismatches between load and photovoltaic generated power and lower for lower mismatches, i.e., The values of IAE, ISE, ITAE and Δf are 0.02375, 0.0005794, 0.01643, and −0.1374 for GA, 0.02201, 0.0003988, 0.01991, and −0.1136 for PSO, 0.022, 0.000409, 0.01936, and −0.1165 for ABC, considering the 0.3394 pu load deviation and 0.01351 pu solar PV power on 1st January in a single-area power system. These values of IAE, ISE, ITAE and Δf are lowered to 0.01587, 0.0002587, 0.01098, and −0.09176 for GA, 0.0147, 0.000178, 0.0133, and −0.07594 for PSO, 0.0147, 0.0001827, 0.01293 and −0.0778 for ABC, for 0.2374 pu load deviation and 0.0147 pu solar PV power on 13th December loading conditions. The values of rise time $T_r(s)$, settling $T_s(s)$, and peak overshoot $M_P(\%)$ remain same for different loading conditions. For example, the values of rise $T_r(s)$, settling $T_s(s)$, and peak overshoot $M_P(\%)$ are 0.0827, 2.55, and 73.4 for GA, 0.0665, 3.03, and 78.4 for PSO, 0.0686, 2.76, and 78.2 for ABC on 1st January loading conditions. FA optimized PID produces relatively poor result as the IAE, ISE, ITAE, and Δf values are much higher than GA, PSO as can be seen the values are 0.07121, 0.005486, 0.04984, and −0.3024.

BESS/PHEV with its different capacities, gain K_B 10 and 50 are taken into consideration. Results depict that settling time $T_s(s)$, peak overshoot $M_P(\%)$ are reduced to 2.04, 63.1 for GA, 2.25, 69.8 for PSO, and 2.3, 69.4 for ABC for K_B of 10. These values are further reduced to 0.94, 29.9 for GA, 1.97, 41.4 for PSO, and 1.75, 40.3 for ABC for K_B of 50. Similarly, the values of IAE, ISE, ITAE and Δf are reduced to 0.01968, 0.0004687, 0.01284, and −0.1302 for GA, 0.01347, 0.0001919, 0.01673, and −0.1092 for PSO,

0.01877, 0.000329, 0.01653, and −0.116 for ABC, for K_B of 10, and further reduced to 0.01412, 0.0002801, 0.009743, and −0.1080 for GA, 0.01475, 0.0001646, 0.01334, and −0.09385 for PSO, 0.01352, 0.0001955, 0.01357, and −0.095 for ABC, for K_B of 50 for 1st January loading conditions. Rise time $T_r(s)$ remains almost unchanged in any case. FA optimized PID produces high error values and frequency deviation although it is connected to BESS/PHEV support. It is concluded that GA optimized produces better results with respect to settling time and peak overshoot but PSO optimized PID produces minimum IAE, ISE, ITAE and Δf using ITAE objective function.

The conventional PID controller is tuned using the PID tuner toolbox within MATLAB. **Tables 6–8** depict that performance indices IAE, ISE, ITAE and Δf increase with the higher load changes and decrease with lower load changes. But rise time $T_r(s)$, settling time $T_s(s)$, and peak overshoot $M_P(\%)$ remains same regardless of the load and photovoltaic power changes. It is depicted that performance indices IAE and ISE decreases when BESS/PHEV is integrated to the system at the gain levels 10 and 50, while ITAE increases when the BESS/PHEV is integrated. Frequency deviation Δf decreases with the attachment of BESS/PHEV support. Rise time $T_r(s)$, settling time $T_s(s)$, and peak overshoot $M_P(\%)$ increase significantly for gain 10, but are infinite at gain 50 because of the unstable response of conventional PID controller. Therefore, the values are replaced by – (dash) where the conventional PID controller response is unstable. It is considered to be major drawback of the conventional PID controller. The conventional PID controller response is shown in **Figures 5–7**.

The maximum steady state frequency deviation permissible limit in Hz is found to be in the range (−0.7932, 0.5468) for maximum positive and negative load deviation respectively. It can be seen from **Table 6**, **Table 7** and **Table 8** that the frequency deviation in Hz has found to be within permissible range using the GA, PSO, ABC, and FA optimization methods. The frequency deviation has not found to be within steady state limit for Conventional PID controller. The frequency deviation range in Hz is (−0.9184, 0.4634) for Conventional-PID. The frequency deviation is suppressed by adding the BESS/PHEV source. But, the PID controller response becomes unstable if the large capacity of BESS/PHEV source is attached to the power system model. The power delivered to power system by BESS and/or PHEV is 0.025 pu for gain K_B of 10, and 0.105 pu for gain K_B of 50 taking into account the maximum positive loading condition on 1st January.

After comparison between the applied techniques and objective functions, it is concluded that PSO optimized PID controller using the ITAE objective function performs well just to mitigate frequency deviation Δf of the power system but GA optimized PID controller using the ISE objective function gives better overall results considering all the performance indices. The convergence characteristics and parameter indices indicate the effectiveness, sustainability and consistency of proposed GA optimized PID tested within the loading range (−0.2275, 0.3394).

CONCLUSION

The load deviation of single area power system and solar photovoltaic power is forecasted using the state-of-the art artificial neural network. PSO, GA, ABC, and FA metaheuristic techniques have been employed to find out the optimal PID controller gain parameters using the IAE, ISE and ITAE objective functions. Some key days, showing significant load changes, have been chosen to see the performance of the single area hybrid power system. Results indicate the efficiency and competency of GA, PSO, and ABC among each other that sufficiently reduce frequency fluctuations. It has been found that PSO optimized PID along with ITAE cost function can sufficiently minimize the frequency. The performance indices and convergence characteristics show overall better results produced from GA optimized PID than others using ISE objective function. These frequency fluctuations are further improved by integrating power from BESS/PHEV source. Small BESS/PHEV capacity is required to damp the frequency when integrated with GA optimized PID.

DATA AVAILABILITY STATEMENT

Publicly available datasets were analyzed in this study. This data can be found here: https://ntdc.gov.pk/services.

AUTHOR CONTRIBUTIONS

SM and AM conceived the conceptualization and methodology. SM conducted the normal analysis and writing. MR and AM conducted the review and editing. MR managed funding acquisition. All authors have agreed to submitted version of the manuscript.

ACKNOWLEDGMENTS

The authors extend their appreciation to the Deputyship for Research and Innovation, Ministry of Education in Saudi Arabia for funding this research work through the project number (IFPIP-1183-135-1442) and King Abdulaziz University, DSR, Jeddah, Saudi Arabia.

REFERENCES

Abd-Elazim, S. M., and Ali, E. S. (2018). Load Frequency Controller Design of a Two-Area System Composing of PV Grid and Thermal Generator via Firefly Algorithm. *Neural Comput. Applic* 30 (2), 607–616. doi:10.1007/s00521-016-2668-y

Abo-Elyousr, F. K. (2018). "Load Frequency Controller with Virtual Inertia Generator for Interconnected Power Systems via Artificial Bee Colony," in 2018 Twentieth International Middle East Power Systems Conference (MEPCON) (Giza, Egypt: IEEE). doi:10.1109/mepcon.2018.8635143

Aditya, S. K., and Das, D. (2001). Battery Energy Storage for Load Frequency Control of an Interconnected Power System. *Electr. power Syst. Res.* 58 (3), 179–185. doi:10.1016/s0378-7796(01)00129-8

Akula, S. K. (2019). *Frequency Control in Microgrid Communities Using Neural Networks*. Wichita, KS, USA: IEEE.

Al-Dahidi, S., Ayadi, O., Alrbai, M., and Adeeb, J. (2019). Ensemble Approach of Optimized Artificial Neural Networks for Solar Photovoltaic Power Prediction. *IEEE Access* 7, 2923905. doi:10.1109/access.2019.2923905

Alessandra, B. A., Carlos Roberto, M., Mara Lucia, M. L., Fábio Roberto, C., and Nelson Jose, P. (2011). Multinodal Load Forecasting in Power Electric Systems Using a Neural Network with Radial Basis Function. *Adv. Mater. Res.* 217, 39. doi:10.4028/www.scientific.net/amr.217-218.39

Azeer, S. A., Ramjug-Ballgobin, R., and Sayed Hassen, S. Z. (2017). Intelligent Controllers for Load Frequency Control of Two-Area Power System. *IFAC-PapersOnLine* 50 (2), 301–306. doi:10.1016/j.ifacol.2017.12.062

Boddepalli, M. K., and Navuri, P. K. (2018). "Design and Analysis of Firefly Algorithm Based PID Controller for Automatic Load Frequency Control Problem," in 2018 Technologies for Smart-City Energy Security and Power (ICSESP) (Bhubaneswar, India: IEEE).

Chandra Sekhar, G. T., Sahu, R. K., Baliarsingh, A. K., and Panda, S. (2016). Load Frequency Control of Power System under Deregulated Environment Using Optimal Firefly Algorithm. *Int. J. Electr. Power & Energy Syst.* 74, 195–211. doi:10.1016/j.ijepes.2015.07.025

Chang, C. S., Fu, W., and Wen., F. (1998). Load Frequency Control Using Genetic-Algorithm Based Fuzzy Gain Scheduling of PI Controllers. *Electr. Mach. Power Syst.* 26 (1), 39–52. doi:10.1080/07313569808955806

Das, D. C., Roy, A. K., and Sinha, N. (2012). GA Based Frequency Controller for Solar Thermal-Diesel-Wind Hybrid Energy Generation/energy Storage System. *Int. J. Electr. Power & Energy Syst.* 43 (1), 262–279. doi:10.1016/j.ijepes.2012.05.025

Das, D. C., Roy, A. K., and Sinha, N. (2010). "Genetic Algorithm Based PI Controller for Frequency Control of an Autonomous Hybrid Generation System," in World Congress on Engineering 2012, July 4-6, 2012 (London, UK: International Association of Engineers). Vol. 2189.

Elsisi, M., Soliman, M., Aboelela, M. A. S., and Mansour, W. (2015). ABC Based Design of PID Controller for Two Area Load Frequency Control with Nonlinearities. *Telkomnika Indonesian J. Electr. Eng.* 16 (1), 58–64. doi:10.11591/tijee.v16i1.1588

Ghasemi, H., and Shayeghi, A. (2011). Market Based LFC Design Using Artificial Bee Colony. *Int. J. Tech. Phys. Problems Eng.* 3 (6), 1–10.

Gozde, H., Cengiz Taplamacioglu, M., and Kocaarslan, İ. (2012). Comparative Performance Analysis of Artificial Bee Colony Algorithm in Automatic Generation Control for Interconnected Reheat Thermal Power System. *Int. J. Electr. Power & Energy Syst.* 42 (1), 167–178. doi:10.1016/j.ijepes.2012.03.039

Gözde, H., Taplamacioğlu, M. C., Kocaarslan, İ., and Çam, E. (2008). Particle Swarm Optimization Based Load Frequency Control in a Single Area Power System. *Sci. Bull.* 2 (8).

Gupta, D. K., Soni, A. K., Jha, A. V., Mishra, S. K., Appasani, B., Srinivasulu, A., et al. (2021). Hybrid Gravitational-Firefly Algorithm-Based Load Frequency Control for Hydrothermal Two-Area System. *Mathematics* 9 (7), 712. doi:10.3390/math9070712

Hazlee Azil, I., Mohamed Zahari, A. F., and Mokhlis, H. (2016). Optimisation of PID Controller for Load Frequency Control in Two-Area Power System Using Evolutionary Particle Swarm Optimisation. *J. Electr. Syst.* 12 (2), 315–324.

Hemeida, A., Mohamed, S., and Mahmoud, M. (2020). Load Frequency Control Using Optimized Control Techniques. *JES. J. Eng. Sci.* 48 (6), 1119–11136. doi:10.21608/jesaun.2020.42349.1011

Hote, Y. V. (2018). PID Controller Design for Load Frequency Control: Past, Present and Future Challenges. *IFAC Pap.* 51, 608. doi:10.1016/j.ifacol.2018.06.162

Huang, C., Bensoussan, A., Edesess, M., and Tsui, K. L. (2016). Improvement in Artificial Neural Network-Based Estimation of Grid Connected Photovoltaic Power Output. *Renew. Energy* 97, 838–848. doi:10.1016/j.renene.2016.06.043

Jaber, A. S., Ahmad, A. Z., and Abdalla, A. N. (2013). An Investigation of Scaled-FLC Using PSO for Multi-Area Power System Load Frequency Control. *Energy Power Eng.* 05 (04), 458–462. doi:10.4236/epe.2013.54b088

Jeyalakshmi, V., and Subburaj, P. (2016). PSO-scaled Fuzzy Logic to Load Frequency Control in Hydrothermal Power System. *Soft Comput.* 20 (7), 2577–2594. doi:10.1007/s00500-015-1659-8

Kalyani, S., Nagalakshmi, S., and Marisha, R. (2012). "Load Frequency Control Using Battery Energy Storage System in Interconnected Power System," in 2012 Third International Conference on Computing, Communication and Networking Technologies (ICCCNT'12) (Coimbatore, India: IEEE). doi:10.1109/icccnt.2012.6396052

Khatoon, S., and Singh, A. K. (2014). "Effects of Various Factors on Electric Load Forecasting: An Overview," in 2014 6th IEEE Power India International Conference (PIICON) (Delhi, India: IEEE). doi:10.1109/poweri.2014.7117763

Konar, G., Mandal, K. K., and Chakraborty, N. (2014). "Two Area Load Frequency Control Using GA Tuned PID Controller in Deregulated Environment," in Proceedings of the International Multi Conference of Engineers and Computer Scientists, 2.

Kotur, D., and Žarković, M. (2016). "Neural Network Models for Electricity Prices and Loads Short and Long-Term Prediction," in 2016 4th International Symposium on Environmental Friendly Energies and Applications (EFEA) (Belgrade, Serbia: IEEE). doi:10.1109/efea.2016.7748787

Kouba, N. E. Y., Menaa, M., Hasni, M., and Boudour, M. (2015). "Optimal Load Frequency Control Based on Artificial Bee Colony Optimization Applied to Single, Two and Multi-Area Interconnected Power Systems," in 2015 3rd International Conference on Control, Engineering & Information Technology (CEIT) (Tlemcen, Algeria: IEEE). doi:10.1109/ceit.2015.7233027

Kumar, D., Mishra, A., and Chatterjee, K. (2017). "Power and Frequency Control of a Wind Energy Power System Using Artificial Bee Colony Algorithm," in 2017 Third International Conference on Science Technology Engineering & Management (ICONSTEM) (Chennai, India: IEEE). doi:10.1109/iconstem.2017.8261385

Kumari, K., Shankar, G., Kumari, S., and Gupta, S. (2016). "Load Frequency Control Using ANN-PID Controller," in 2016 IEEE 1st International Conference on Power Electronics, Intelligent Control and Energy Systems (ICPEICES) (Delhi, India: IEEE). doi:10.1109/icpeices.2016.7853516

Kumari, N., and Jha, A. N. (2014). Frequency Response Enhancement of Hybrid Power System by Using PI Controller Tuned with PSO Technique. *Int. J. Adv. Comput. Res.* 4 (1), 116.

Liang, L., Jin, Z., and Jiao, Z. (2012). "Frequency Regulation for a Power System with Wind Power and Battery Energy Storage," in 2012 IEEE International Conference on Power System Technology (POWERCON) (Auckland, New Zealand: IEEE). doi:10.1109/powercon.2012.6401357

Lone, A. H., Yousuf, V., Prakash, S., and bid Bazaz, M. A. (2018). "Load Frequency Control of Two Area Interconnected Power System Using SSSC with PID, Fuzzy and Neural Network Based Controllers," in 2018 2nd IEEE International Conference on Power Electronics, Intelligent Control and Energy Systems (ICPEICES) (Delhi, India: IEEE). doi:10.1109/icpeices.2018.8897468

Mallesham, G., Mishra, S., and Jha, A. N. (2012). "Automatic Generation Control of Microgrid Using Artificial Intelligence Techniques," in 2012 IEEE Power and Energy Society General Meeting (San Diego, CA, USA: IEEE).

MathWorks (2022). *PID Controller Tuning in Simulink*. Available at: https://www.mathworks.com/help/slcontrol/gs/automated-tuning-of-simulink-pid-controller-block.html.

MathWorks (2022). *PID Tuner*. Available at: https://www.mathworks.com/help/control/ref/pidtuner-app.html.

Mellit, A., and Pavan, A. M. (2010). Performance Prediction of 20kWp Grid-Connected Photovoltaic Plant at Trieste (Italy) Using Artificial Neural Network. *Energy Convers. Manag.* 51, 2431–2441. doi:10.1016/j.enconman.2010.05.007

Milani, A. E., and Mozafari, B. (2009). Genetic Algorithm Based Optimal Load Frequency Control in Two-Area Interconected Power Systems. *AIP Conf. Proc.* 1159 (1), 43. doi:10.1063/1.3223953

Modi, N., Khare, M., and Chaturvedi, K. (2013). Performance Analysis of Load Frequency Control in Single Area Power System Using GA and PSO Based PID Controller. *Int. J. Electr. Electron. Comput. Eng.* 2 (1), 108–114.

Mosaad, M. I., and Salem., F. (2014). LFC Based Adaptive PID Controller Using ANN and ANFIS Techniques. *J. Electr. Syst. Inf. Technol.* 1 (3), 212–222. doi:10.1016/j.jesit.2014.12.004

Nagarjuna, N., and Shankar, G. (2015). "Load Frequency Control of Two Area Power System with AC-DC Tie Line Using PSO Optimized Controller," in 2015 International Conference on Power and Advanced Control Engineering (ICPACE) (Bengaluru, India: IEEE). doi:10.1109/icpace.2015.7274948

Naidu, K., Mokhlis, H., and Bakar, A. H. A. (2013). "Application of Firefly Algorithm (FA) Based Optimization in Load Frequency Control for Interconnected Reheat Thermal Power System," in 2013 IEEE Jordan Conference on Applied Electrical Engineering and Computing Technologies (AEECT) (Amman, Jordan: IEEE). doi:10.1109/aeect.2013.6716461

Naidu, K., Mokhlis, H., and Bakar, A. H. A. (2014). Multiobjective Optimization Using Weighted Sum Artificial Bee Colony Algorithm for Load Frequency Control. *Int. J. Electr. Power & Energy Syst.* 55, 657–667. doi:10.1016/j.ijepes.2013.10.022

Ncane, Z. P., and Saha, A. K. (2019). "Forecasting Solar Power Generation Using Fuzzy Logic and Artificial Neural Network," in 2019 Southern African Universities Power Engineering Conference/Robotics and Mechatronics/Pattern Recognition Association of South Africa (SAUPEC/RobMech/PRASA) (Bloemfontein, South Africa: IEEE). doi:10.1109/robomech.2019.8704737

Newkirk, M. (2015). What Is A Hybrid Solar System? Available at: https://www.cleanenergyreviews.info/blog/2014/8/14/what-is-hybrid-solar.

Otani, T. (2017). "Cooperative Load Frequency Control of Generator and Battery Using a Recurrent Neural Network," in Proc. of the 2017 IEEE Region 10 Conference (TENCON) (Malaysia: TENCON), 918–923. doi:10.1109/tencon.2017.8227989

Padhan, S., Sahu, R. K., and Panda, S. (2014). Application of Firefly Algorithm for Load Frequency Control of Multi-Area Interconnected Power System. *Electr. power components Syst.* 42 (13), 1419–1430. doi:10.1080/15325008.2014.933372

Pain, S., and Acharjee, P. (2014). Multiobjective Optimization of Load Frequency Control Using Pso. *Int. J. Emerg. Technol. Adv. Eng.* 4 (7), 16–22.

Power Data Reference Book (2017). *Power Data Reference Book, Vol 2, 2010-11 to 2016-17*. Lahore: Planning Power National Transmission and Despatch Company Limited (NTDCL). Available at: https://ntdc.gov.pk/services.

Prajapati, P., and Parmar, A. (2016). "Multi-area Load Frequency Control by Various Conventional Controller Using Battery Energy Storage System," in 2016 International Conference on Energy Efficient Technologies for Sustainability (ICEETS) (Nagercoil, India: IEEE). doi:10.1109/iceets.2016.7583800

Prakash, S., and Sinha, S. K. (2012). "Four Area Load Frequency Control of Interconnected Hydro-Thermal Power System by Intelligent PID Control Technique," in 2012 Students Conference on Engineering and Systems (Allahabad, India: IEEE). doi:10.1109/sces.2012.6199090

Qi, X., Bai, Y., Luo, H., Zhang, Y., Zhou, G., and Wei, Z. (2018). Fully-distributed Load Frequency Control Strategy in an Islanded Microgrid Considering Plug-In Electric Vehicles. *Energies* 11 (6), 1613. doi:10.3390/en11061613

Rao, C. S. (2012). Design of Artificial Intelligent Controller for Automatic Generation Control of Two Area Hydrothermal System. *Int. J. Electr. Comput. Eng.* 2 (2), 183.

Rao, R. N., and Rama Krishna Reddy, P. (2015). PSO Based Tuning of PID Controller for a Load Frequency Control in Two Area Power System. *Int. J. Eng. Res. Appl.* 1 (3), 1499–1505.

Rathor, S., Acharya, D. S., Gude, S., and Mishra, P. (2011). "Application of Artificial Bee Colony Optimization for Load Frequency Control," in 2011 World Congress on Information and Communication Technologies (Mumbai, India: IEEE). doi:10.1109/wict.2011.6141339

Regad, M., Helaimi, M., Taleb, R., Gabbar, H. A., and Othman, A. M. (2019). "Fractional Order PID Control of Hybrid Power System with Renewable Generation Using Genetic Algorithm," in 2019 IEEE 7th International Conference on Smart Energy Grid Engineering (SEGE) (Oshawa, ON, Canada: IEEE). doi:10.1109/sege.2019.8859970

Rerkpreedapong, D., Hasanovic, A., and Feliachi, A. (2003). Robust Load Frequency Control Using Genetic Algorithms and Linear Matrix Inequalities. *IEEE Trans. Power Syst.* 18 (2), 855–861. doi:10.1109/tpwrs.2003.811005

Rodríguez, F., Fleetwood, A., Galarza, A., and Fontán, L. (2018). Predicting Solar Energy Generation through Artificial Neural Networks Using Weather Forecasts for Microgrid Control. *Renew. energy* 126, 855–864. doi:10.1016/j.renene.2018.03.070

Sadat, H. (2012). *Power System Analysis and Design*, 33–41.

Safari, A., Babaei, F., and Farrokhifar, M. (2021). A Load Frequency Control Using a PSO-Based ANN for Micro-grids in the Presence of Electric Vehicles. *Int. J. Ambient Energy* 42 (6), 688–700. doi:10.1080/01430750.2018.1563811

Sedaghati, F., Nahavandi, A., Ali Badamchizadeh, M., Ghaemi, S., and Abedinpour Fallah, M. (2012). PV Maximum Power-point Tracking by Using Artificial Neural Network. *Math. Problems Eng.* 2012, 506709. doi:10.1155/2012/506709

Selvakumaran, S., Parthasarathy, S., Karthigaivel, R., and Rajasekaran, V. (2012). Optimal Decentralized Load Frequency Control in a Parallel AC-DC Interconnected Power System through HVDC Link Using PSO Algorithm. *Energy Procedia* 14, 1849–1854. doi:10.1016/j.egypro.2011.12.1178

Shakarami, M. R., Faraji, I., Asghari, I., and Akbari, M. (2013). "Optimal PID Tuning for Load Frequency Control Using Lévy-Flight Firefly Algorithm," in 2013 3rd International Conference on Electric Power and Energy Conversion Systems (Istanbul, Turkey: IEEE). doi:10.1109/EPECS.2013.6713008

Shankar, G., Lakshmi, S., and Nagarjuna, N. (2015). "Optimal Load Frequency Control of Hybrid Renewable Energy System Using PSO and LQR," in 2015 International Conference on Power and Advanced Control Engineering (ICPACE) (Bengaluru, India: IEEE). doi:10.1109/icpace.2015.7274942

Sidi Brahim, R. M., M'hamed, H., Taleb, R., and Lemrabout, A. (2021). Load Frequency Control of Hybrid Power System Using Classical PID Controller. *iKSP J. Comput. Sci. Eng.* 1 (1).

Singh, R, and Ramesh, L. (2019). Comparison of Automatic Load Frequency Control in Two Area Power Systems Using Pso Algorithm Based Pid Controller and Conventional Pid Controller. *J. Phys. Conf. Ser.* 1172, 012054. doi:10.1088/1742-6596/1172/1/012054

Srinivasan, D., Liew, A. C., and Chen, J. S. P. (1991). "Short Term Forecasting Using Neural Network Approach," in Proceedings of the First International Forum on Applications of Neural Networks to Power Systems (Piscataway, NJ, USA: IEEE).

Sundaram, V. S., and Jayabarathi, T. (2011). "Load Frequency Control Using PID Tuned ANN Controller in Power System," in 2011 1st International Conference on Electrical Energy Systems (Chennai, India: IEEE). doi:10.1109/icees.2011.5725341

Taher, S. A. (2014). Fractional Order PID Controller Design for LFC in Electric Power Systems Using Imperialist Competitive Algorithm. *Ain Shams Eng. J.* 5, 133–135. doi:10.1016/j.asej.2013.07.006

Takagi, M., Yamamoto, H., Yamaji, K., Okano, K., Hiwatari, R., and Ikeya, T. (2009). Load Frequency Control Method by Charge Control for Plug-In Hybrid Electric Vehicles with LFC Signal. *IEEJ Trans. Power Energy* 129 (11), 1342–1348. doi:10.1541/ieejpes.129.1342

Uehara, A., Senjyu, T., Yona, A., and Funabashi, T. (2009). "Frequency Control by Coordination Control of WTG and Battery Using Load Estimation," in 2009 International Conference on Power Electronics and Drive Systems (PEDS) (Taipei, Taiwan: IEEE). doi:10.1109/peds.2009.5385765

Veerasamy, V., Wahab, N. I. A., Ramachandran, R., Othman, M. L., Hizam, H., Irudayaraj, A. X. R., et al. (2020). A Hankel Matrix Based Reduced Order Model for Stability Analysis of Hybrid Power System Using PSO-GSA Optimized Cascade PI-PD Controller for Automatic Load Frequency Control. *IEEE Access* 8, 71422–71446. doi:10.1109/access.2020.2987387

Yang-Wu, S., Xun, M., Ao, P., Yang-Guang, W., Ting, C., Ding, W., et al. (2019). "Load Frequency Control Strategy for Wind Power Grid-Connected Power Systems Considering Wind Power Forecast," in 2019 IEEE 3rd Conference on Energy Internet and Energy System Integration (EI2) (Changsha, China: IEEE). doi:10.1109/EI247390.2019.9062084

Conflict of Interest: The authors declare that the research was conducted in the absence of any commercial or financial relationships that could be construed as a potential conflict of interest.

Publisher's Note: All claims expressed in this article are solely those of the authors and do not necessarily represent those of their affiliated organizations, or those of the publisher, the editors and the reviewers. Any product that may be evaluated in this article, or claim that may be made by its manufacturer, is not guaranteed or endorsed by the publisher.

APPENDIX

The typical values for the hybrid power system are given below

$P_r = 219MW, f = 50Hz, H = 5, D = 0.8, \tau_g = 10\ sec, \tau_t = 5\ sec,\ R = 0.05\ Hz/_{pu.MW}$,

$\tau_{charge} = 100, \tau_{conv} = 0.02, K_B = 10\&50, K_{pb} = -0.02$

NOMENCLATURE

IAE Integral absolute error

ISE Integral square error

ITAE Integral time absolute error

GA Genetic algorithm

PSO Particle swarm optimization

ABC Artificial bee colony

FA Firefly algorithm

$T_r\,(s)$ Rise time

$T_s\,(s)$ Settling time

$M_P\,(\%)$ Peak overshoot

$\Delta f\,(Hz)$ Maximum frequency deviation in Hertz

K_p Proportional gain

K_i Integral gain

K_d Derivative gain

ACE Area control error

ΔP_m Change in mechanical power

ΔP_{PV} Solar photovoltaic power

ΔP_e Net change in electrical load demand

$\mathbf{P_{BESS/PHEV}}$ Battery Energy Storage System/Plug—in Hybrid Electric Vehicle Power

K_B BESS/PHEV gain

τ_{conv} DC-AC converter time constant

τ_{charge} BESS/PHEV charging time constant

$\mathbf{P_{rated}}$ Rated power plant power

$\Delta \mathbf{f}$ Change in nominal frequency

H Generator inertia constant

$\Delta \mathbf{P_L}$ Change in frequency sensitive load power

$\boldsymbol{\tau_t}$ Turbine time constant

$\boldsymbol{\tau_g}$ Governor time constant

$\mathbf{D} = \frac{\Delta \mathbf{P_L}}{\Delta \mathbf{f}}$ Ratio of percent change in load to percent change in frequency

R Governor speed regulation per unit

β Attractiveness parameter

γ Coefficient of absorption